UNIVERSITY OF OKLAHOMA

GRADUATE COLLEGE

A FUZZY LOGIC ALGORITHM FOR CLASSIFYING BIRD AND INSECT RADAR ECHOES AT S-BAND

A THESIS

SUBMITTED TO THE GRADUATE FACULTY

in partial fulfillment of the requirements for the

Degree of

MASTER OF SCIENCE

By

PRECIOUS JATAU
Norman, Oklahoma
2018

Downloaded from SHAREOK. Persistent Handle URL: https://hdl.handle.net/11244/301344

A FUZZY LOGIC ALGORITHM FOR CLASSIFYING BIRD AND INSECT RADAR ECHOES AT S-BAND

A THESIS APPROVED FOR THE
SCHOOL OF ELECTRICAL AND COMPUTER ENGINEERING

BY

_____
Dr. Tian-You Yu, Chair

_____
Dr. Valery Melnikov

_____
Dr. Joseph Havlicek

© Copyright by PRECIOUS JATAU 2018
All Rights Reserved.

Table of Contents

List of Tables vi
List of figures vii
Abstract ix
Chapter 1 1
Introduction 1
Chapter 2 7
Literature Review 7
2.1 Radar Cross Section 8
2.2 Important Radar Parameters 10
2.3 Simple Radar Equation and Signal Model 13
2.4 Weather Radar Equation 15
2.5 NEXRAD 18
2.6 NEXRAD level II products 21
2.6.1 Reflectivity Z 21
2.6.2 Velocity V 22
2.6.3 Spectrum Width $\boldsymbol{\sigma_V}$ 23
2.6.4 Differential Reflectivity Z_{DR} 23
2.6.5 Differential Phase $\boldsymbol{\varphi_{DP}}$ 23
2.6.6 Cross Correlation Coefficient $\boldsymbol{\rho_{HV}}$ 24
2.7 Clear Air Echoes 25
2.7.1 Nature/Origin of Clear Air Echoes 25
2.7.2 Characteristics of Clear Air Echoes 27
2.7.3 Nocturnal Clear Air Echoes 30
2.7.4 Day Time Clear Air Echoes 31
2.8 Classifying Birds vs Insects 33
Chapter 3 35
Procedure 35
3.1 Data Collection 35
3.1.1 Selection of Clear Air Days 36
3.1.2 KTLX Collection Mode 38

3.2 Data Processing 41
3.2.1 Data Preprocessing 42
3.2.2 Texture 43
3.2.3 Thirty Minute Data Processing 44
3.3 Results 45
3.3.1 Reflectivity Z 45
3.3.2 Velocity V 45
3.3.3 Spectrum Width $\boldsymbol{\sigma_V}$ 46
3.3.4 Differential Reflectivity Z_{DR} 46
3.3.5 Differential Phase $\boldsymbol{\varphi_{DP}}$ 46
3.3.6 Correlation Coefficient $\boldsymbol{\rho_{HV}}$ 47
3.3.7 Velocity Texture $\boldsymbol{\Delta V}$ 47
3.3.8 Spectrum Width Texture $\boldsymbol{\Delta\sigma_V}$ 47
3.3.9 Other texture parameters 48
Chapter 4 61
Fuzzy Logic Algorithm to distinguish bird and insect radar echoes 61
4.1 Introduction 61
4.2 General structure of the algorithm 62
4.3 Membership functions and Weights 65
4.4 Classification Results 72
4.4.1 Insect Case 72
4.4.2 Daily Cycle Case 72
Chapter 5 80
Summary and Conclusions 80
References 85

List of Tables

Table 1. 1 Bird strikes reported by US airports between 2011 – 2014 ……... 5

Table 2. 1 Specifications of WSR-88 D 20

Table 4. 1 Weights of all variables and ranges..... 71

List of Figures

Fig. 1. 1 Hudson Landing of flight 1549 caused by engine shut down due to bird strike (Source: CNN) 3
Fig. 1. 2 Damaged aircraft cockpit by bird strikes. 4
Fig. 1. 3 Damaged aircraft engine by a bird strike. (Wikipedia, 2009) 4

Fig. 2. 1The Mie curve shows RCS vs diameter of sphere (Stepanian, et al., 2016) 10
Fig. 2. 2 NEXRAD coverage of Contiguous US. Retrieved from (NOAA's National Weather Service Radar Operations Center, n.d.) 19
Fig. 2. 3 Calculation of φDP for three distinct pulses. Retrieved from (Dual-Polarization Radar Principles and Systems Operations, 2018) 24
Fig. 2. 4 Average Reflectivity below 2 km versus time for a nocturnal case. Sunset is at 2Z and Sunrise is at 11Z. Data is from Cimarron radar collected May 31, 1999. (Martin, 2003) 28

Fig. 3. 1 Street View of KTLX WSR-88D radar 37
Fig. 3. 2 Satellite View of KTLX radar 37
Fig. 3. 3 Mesonet Sounding for September 2017 38
Fig. 3. 4 PPI plots showing data from Day Time (20:00 UTC). WSR-88 D KTLX, 4 Sept, 2017 40
Fig. 3. 5 Same as fig 3.4 but for Midnight 5th Sept, 2017 40
Fig. 3. 6 Flow chart of the data processing algorithm 42
Fig. 3. 7 Set-up for calculating texture at gate 0 43
Fig. 3. 8 Distribution of Z for clear air days in September 2017. 49
Fig. 3. 9 Same as 3.8 but for V 50
Fig. 3. 10 Distribution of σ_V for Clear Air Days in September 2017 51
Fig. 3. 11 Distribution of Z_{DR} for Clear Air Days in September 2017 52
Fig. 3. 12 Distribution of φ_{DP} for Clear Air Days in September 2017 53
Fig. 3. 13 Distribution of ρ_{HV} for Clear Air Days in September 2017 54
Fig. 3. 14 Velocity texture ΔV 55
Fig. 3. 15 Spectrum Width texture $\Delta\sigma_V$ 56
Fig. 3. 16 Histogram of ΔZ for Clear Air Days in September 2017 57
Fig. 3. 17 Z_{DR} texture ΔZ_{DR} 58
Fig. 3. 18 φDP texture $\Delta\varphi_{DP}$ 59
Fig. 3. 19 ρHV texture $\Delta\rho_{HV}$ 60

Fig. 4. 1 Flow chart of fuzzy logic algorithm 63
Fig. 4. 2 Membership functions for ΔV 67
Fig. 4. 3 Membership functions for $\Delta\sigma_V$ 67
Fig. 4. 4 Membership functions for φ_{DP} 68
Fig. 4. 5 Membership functions for ρ_{HV} 68

Fig. 4. 6 Membership functions for σ_V 69
Fig. 4. 7 Membership functions for Z_{DR} 69
Fig. 4. 8 Membership functions for Z 70
Fig. 4. 9 Area of Overlapping region for φ_{DP} for 40 – 50 km 71
Fig. 4. 10 Classification result for 19th July, 2013 at 12:46:04 CDT. 74
Fig. 4. 11 Classification result for 1st November, 2013 at 17:30:06 CDT 75
Fig. 4. 12 Classification result for 19 CDT, 16 September, 2015 to 1 CDT, 17 September, 2015 76
Fig. 4. 13 Classification result for 17 Sept, 2015, 1 CDT to 6 CDT 77
Fig. 4. 14 Same as 4.13 but for 7 CDT to 12 CDT 78
Fig. 4. 15 Same as 4.14 but for 13 CDT to 18 CDT 79

Abstract

A fuzzy logic algorithm for the separation of bird echoes from insect echoes using Next Generation Radar (NEXRAD) and considering range effects has been developed. The radar used in this study is the S-band (10 cm wavelength) KTLX WSR-88D radar located in Oklahoma City. Insects are known to dominate day time clear air echoes while birds dominate nocturnal echoes during migration season. September has also been found to be peak migrating season for birds. Data was analyzed from all clear air days in September 2017 to verify the composition of clear air echoes. Results confirm insect (bird) dominance during day (night). Also, the membership functions are derived directly from the distributions of radar variables and weighted in an objective manner. Finally, the algorithm is tested on three cases. Two cases with known Monarch butterfly abundance, confirmed by the US Department of Agriculture (USDA) are correctly identified as being insect dominated. One final classification for a 24-hour period further confirms that birds (insects) are responsible for most night (day) time radar echoes.

Chapter 1

Introduction

Weather radars are designed to monitor severe weather and measure precipitation. The USA network of Weather Surveillance 1988 Doppler Radars, WSR-88D consists of 160 systems deployed across the continental US, Alaska, and in Puerto Rico. Sensitivity of the radars are sufficient to observe echoes from insects, birds, and bats. The WSR-88D classify such echoes as biological scatters without distinguishing the taxa. Distinguishing radar echoes from birds and insects is important for weather observations, aviation, ecology, agriculture, and biology.

Bird strikes are a major hazard for aviation. They are defined by the Federal Aviation Authority (FAA) as collisions between a bird and an aircraft resulting in the injury/death of the bird, damage of the aircraft or both. (Seidenman & Spanovich, 2016). Perhaps the most high-profile incident occurred on 15 January 2009. The US Airways Flight 1549 encountered a flock of Canada Geese shortly after takeoff from the New York City LaGuardia Airport. Some birds were ingested into both engines leading to a shut down and loss of thrust. Luckily, the pilot was on the day was Captain Chesley Sullenberger, who had decades of experience flying military and civilian aircraft. He successfully landed the plane on the Hudson River (shown in fig. 1.1) saving the lives of all 155 people on board. However, not all bird strike incidents can be redeemed by the expertise of a veteran pilot. Many bird strikes have caused deaths and damage of aircraft.

According to the National Wildlife Strike Database (Federal Aviation Administration, 2016), the number of strikes annually reported has increased 7.4 times from 1,847 in 1990 to a record 13,795 in 2015. Within this timeframe, 169,856 strikes were reported either as happened in the USA or by U.S registered aircraft in foreign countries. The 2015 total of 13,795 strikes saw an increase by 103 strikes (1 percent) compared to 13,692 strikes reported in 2014. Birds accounted for 95.8 percent of the 2015 reported strikes. Table 1.1 presents the number of bird strikes reported by the U.S airports in 2011 – 2014.

Although, there is a substantial risk of aircraft bird strike being to the windshield, nose, wing/rotor and radome, Engines sustained the highest percentage of damage of major components. Fig 1.2 and 1.3 below show bird damaged aircraft cockpit and engine. The FAA reports that in 1990-2015, there were 16,636 cases of bird strikes on engines of which 27 percent resulted in damage. About 5 percent of damaged engines required removal. (Seidenman & Spanovich, 2016). Globally wildlife strikes have killed more than 262 people and destroyed over 247 aircraft since 1988. The annual cost of wildlife strikes to the USA aviation industry in 2015 is estimated to be at least $229 million in direct and other monetary losses. This is a huge loss of resource to the United States.

The trend of bird strikes is expected to increase because of a growth in the population of large birds and increasing air traffic. Out of 30 species of birds found to frequently strike aircraft, it was found for every 100g increase in body mass, there was a 1.26% increase in the likelihood of damage. As such large birds like geese, pelicans, cranes and eagles are especially dangerous. Several methods currently exist for wildlife

management around airports. They include habitat management, technology for deterring wild life species, sound systems to keep birds away from take-off/landing areas, satellite telemetry and other animal tracking techniques. Mounted lighting systems are also used to illuminate aircrafts so that incoming birds can easily detect and avoid them. While all these methods are effective for tracking/repelling birds, they do not provide the continental scale continuous surveillance of the NEXRAD network. An algorithm for detecting birds using NEXRAD would immensely improve aviation safety. As such, the main goal of this thesis is to develop an algorithm that detects the presence of birds in the terminal region of an airport.



Fig. 1. 1 Hudson Landing of flight 1549 caused by engine shut down due to bird strike (Source: CNN)

Distinguishing birds and insects is also important for meteorology, agriculture and biology. Insects are perfect wind tracers because of their lower mass and passive

flight. Birds on the other hand have a heavier mass and are active fliers. They have been found to bias wind measurements with their flight velocities. (Wilczak, et al., 1995).



Fig. 1. 2 Damaged aircraft cockpit by bird strikes.

(Patterson, 2016) (Seidenman & Spanovich, 2016)



Fig. 1. 3 Damaged aircraft engine by a bird strike. (Wikipedia, 2009)

Identifying radar echoes from insects and birds can improve the accuracy of radar derived winds. Furthermore, many insect species are agricultural pests. They feed on plants reducing the yield. Integrated pest management (IPM) techniques seeks to address this problem, by ascertaining the presence, abundance and distribution of these insects before taking environmentally sensitive measures to reduce the insect population

(Zehnder, 2014). Ornithologist also study radar patterns to understand large scale bird behavior.

The Top 10 U.S. Airports for Reported Bird Strikes, 2011-14

Denver Intl. Airport	1,830
Dallas/Fort Worth Intl. Airport	1,482
Chicago O'Hare Intl. Airport	982
Philadelphia Intl. Airport	844
John F. Kennedy Intl. Airport	829
Salt Lake City Intl. Airport	762
Memphis Intl. Airport	746
Orlando Intl. Airport	666
LaGuardia Airport	616
Total Reported Globally	**65,139**

Table 1.1 Bird strikes reported by US airports between 2011 – 2014. Adopted from (Seidenman & Spanovich, 2016)

The WSR-88D is a very sensitive system. It can detect a small single bird at distances up to 100 km from radar. Most probable times of bird strikes are periods of bird migration. Birds migrate intensely at fair weather, which is called "clear air" in radar meteorology. In "clear air" situations, no precipitation is observed, but radar can show large echoes from birds, bats, and insects, which is called atmospheric biota. Birds and insects produce very similar echoes in clear air. Birds typically migrate at night when there can be some nocturnal insects. In the day time, some species of birds forage on insects. While birds dominate night radar echoes and vice versa, both species should be expected to be found at any time of the day.

The mixture of species in the atmosphere creates difficulty in knowing exactly what is being studied. Assumptions by Meteorologists might be used in Ornithological or Entomological studies. This leaves a lot of ambiguity about the exact specie being observed. It is possible ornithologists accidentally study insects while Entomologists could mistakenly study birds. Furthermore, most clear air studies are based on reflectivity which is highly variable depending on radar cross section and abundance of scatterers in the atmosphere. It is of utmost importance that a more robust method for delineating clear air echoes is developed. Current algorithms like The Hydrometeor Classification Algorithm currently used on the NEXRAD network defines a broad biological class of echoes (Park, 2008), without identifying the taxa.

This thesis seeks to properly characterize two classes of biological echoes: birds and insects. First, clear air data from bird migration season collected by the WSR 88D, KTLX radar are analyzed to verify features of these echoes. Finally, a fuzzy logic algorithm for classifying bird and insect echoes in clear air is developed and tested. The algorithm has the potential to be applied on the NEXRAD network. The next chapter presents a review of radar theory, NEXRAD, level II products and the source of clear air echoes. Data collection, analysis and results for each taxa are discussed in Chapter 3. Finally, the fuzzy logic algorithm and test results are discussed in Chapter 4 followed by summary and conclusions in Chapter 5.

Chapter 2

Literature Review

The name RADAR is an acronym which summarizes the basic functions of the system: RADio Detection And Ranging. Perhaps the earliest mention of the radar concept was by Nikola Tesla in 1900 who said “When we raise the voice and hear an echo in reply, we know that the sound of the voice must have reached a distant wall, or boundary, and must have been reflected from the same. Exactly as sound, so an electrical wave is reflected……we may determine the relative position or course of a moving object such as a vessel at sea, the distance travelled by the same or its speed ” (Doviak & Zrnic, 1993). Radars as we know them today operate on this fundamental principle. Radar detect targets by transmitting a radio wave and analyzing the received echo. It can operate day and night and in all weather conditions.

A pulsed doppler radar transmits a pulse instead of a continuous wave. Pulsed Doppler radars were developed during WW2 to improve the detection of aircraft and moving objects in the presence of clutter from sea and land (Doviak & Zrnic, 1993). Over time, Pulsed Doppler radars have evolved into sensitive systems capable of detecting weather echoes. The NEXRAD (Next generation Radar) network consists of 160 pulse Doppler radars with dual polarization, used for weather surveillance across the US, Alaska, Hawaii and Puerto Rico. It is a system that consists of the WSR-88D radars (Weather Surveillance Radar – 1988 Doppler), radar data acquisition (RDA) and radar product generator (RPG) subsystems, and a dedicated network for collecting data.

Basic pulse doppler radars measure the range, power, radial velocity and direction of targets. NEXRAD produces 6 products: reflectivity (Z), radial velocity (V), and spectrum width (σ_V) from the horizontal polarization as well as differential reflectivity (Z_{DR}), differential phase (ϕ_{DP}) and correlation coefficient (ρ_{HV}) using both polarizations. These products provide information about the size, velocity, uniformity of motion, shape, content and diversity of targets in a resolution volume. They are crucial to our ability to separate echoes from birds and insects, hence it is necessary to discuss how they are generated. This chapter is organized as follows: first, an overview of the basic operation of the radar from pulse transmission to product generation is provided. Next, a detailed description of each product is presented followed by a review of "clear air" studies. Finally, the case is presented for why daytime echoes are mostly caused by insects while nocturnal echoes are caused by birds.

2.1 Radar Cross Section

When an incident radar wave interacts with a target, part of the power is scattered back to the radar receiver. Radar cross section is the equivalent area of a dielectric sphere that would reflect the same power as that target. Radar cross section (RCS) is sensitive to many properties of the target like its orientation relative to the radar beam, material, shape and size. It also depends on the wavelength and polarization of the incident wave. A famous theory developed by Gustav Mie (1908) describes the back-scattering area for dielectric spheres as a function of its diameter. The results are presented as the so-called Mie curve shown in fig 2.1 (Stepanian et al., 2016). Four scenarios (labelled A - D) for distinct sphere sizes are considered, shown on the left of

fig 2.1. Their corresponding radar cross section are also noted on the Mie curve. There are three main regions: the Rayleigh, resonant and optical regions.

The Rayleigh region describes scattering of targets that are much smaller than the radar wavelength. The diameter D of the dielectric sphere is in the interval D $<\frac{\lambda}{16}$, (approx. 6.25 mm for NEXRAD, for the wavelength λ = 10 cm), such that it can be considered to have one phase center upon scattering. When the target interacts with an incident wave, it radiates back a wave with a constant phase shift. Therefore, RCS increases with the physical size of scatterers. RCS is proportional to D^6 and approximates the real sphere size (Doviak & Zrnic, 1993). It is given by

$$\sigma_{Ray} = \frac{\pi^5}{\lambda^4}|K|^2 D^6 \quad , \tag{2.1}$$

where K is a function of index of refraction and absorption of water defined as

$$K = \frac{(m^2-1)}{(m^2+2)} \quad , \tag{2.2}$$

where *m* is the complex index of refraction

For water at microwave wavelengths $|K|^2$ is about 0.93. Some small insect species observed from any aspect would fall in the Rayleigh region.

As the sphere diameter increases, scattering can be considered as reflections from many Rayleigh scatterers with distinct phase centers. The incident wave interacts with these phase centers to scatter back several waves with distinct phases. They might initially interfere destructively leading to the first local minima of RCS at point C in the Mie curve (fig. 2.1). As the size further increases (scenario D), phases of the scattered

waves align better leading to an increased RCS. This pattern repeats causing the radar cross section to oscillate as a function of the sphere size. As such, this region is called the resonance region. Some birds and some insects observed with NEXRAD fall in this region and therefore have a highly variable radar cross section. This means their Reflectivity, which is a function of target's RCS would also vary.

In the optical region, the sphere is much larger than the radar wavelength. Internal inhomogeneities caused by scattering of various parts of the sphere average out leading to a proportional increase in RCS as the sphere diameter expands.

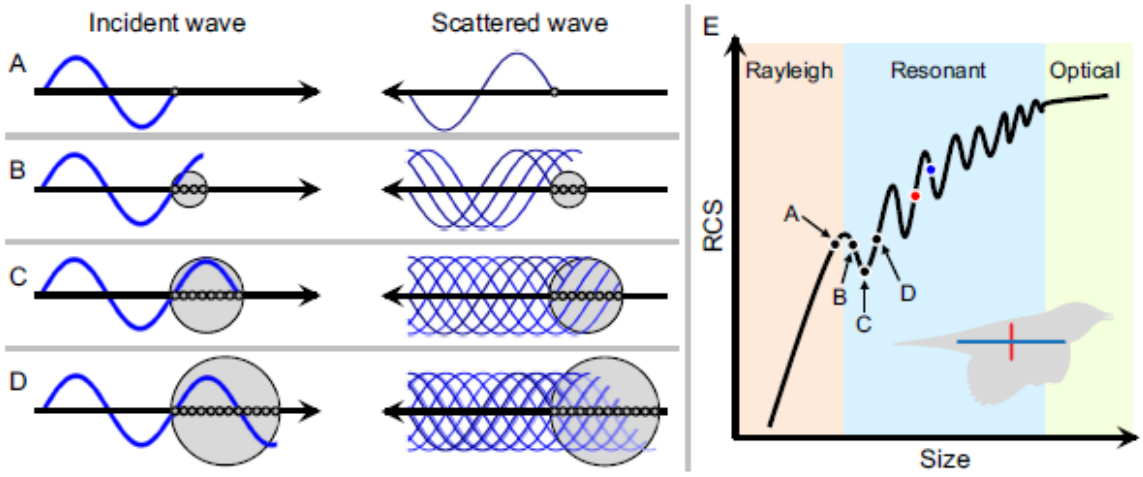

Fig. 2. 1 The Mie curve shows radar cross section vs diameter of sphere (Stepanian, et al., 2016)

2.2 Important Radar Parameters

Skolnik (2001) presents a good introduction to radar system parameters. When a pulse Doppler radar transmits a short burst of radiation toward a target at range R, the

received echo is delayed by a time T_R. Target range is the spatial equivalent of delay T_R expressed as

$$R = \frac{cT_R}{2} \quad , \tag{2.3}$$

where c is the speed of light.

Scatterers also produce measurable Doppler shifts when illuminated with a radar beam. Incident radiation on the scatterer creates electromagnetic vibrations which are measured as the frequency of the received signal. If the scatterer is stationary, it vibrates at the frequency of the transmit wave. A scatterer approaching the radar will vibrate at a higher frequency because it sees the transmit wave as propagating at a higher speed. Similarly, a receding scatterer will reflect a signal at a slower frequency. Doppler frequency f_D is the shift between the frequency of the transmitted and received signal. It is expressed as

$$f_D = \frac{2V}{\lambda} \quad , \tag{2.4}$$

where V is the radial velocity, and λ is the radar wavelength.

Several considerations are made in defining the parameters of a radar system. Range resolution ΔR is the minimum distance between two scatterers within which their received echoes are separable. Radar pulse duration τ is usually chosen based on the desired range resolution given by the relationship

$$\Delta R = \frac{c\tau}{2} \quad . \tag{2.5}.$$

Furthermore, to improve Signal to Noise Ratio (SNR) of variables, radar transmits several pulses and averages their received waveform. The delay between successive samples is called the Pulse Repetition Time (PRT), T_p. Radar sampling can also be thought of in terms of the Pulse Repetition Frequency, $f_p = \frac{1}{T_p}$. At the transit of every new pulse, the radar resets its clock to measure delay caused by targets. Thus, when the echoes from a previous pulse arrives after a new pulse has been sent out, radar measures an apparent delay of $T_R - mT_p$ subsequently causing aliasing of detected range (m is the largest positive integer such that $T_R \geq mT_p$). To mitigate the effect of range aliasing a wide T_p is desired. The radar's maximum unambiguous range R_{un} is expressed as

$$R_{un} = \frac{cT_p}{2} \quad , \tag{2.6}$$

On the other hand, the accuracy of velocity estimation depends on collecting many pulses over a short T_p. The maximum unambiguous velocity V_{un} is the highest unaliased velocity the radar can measure. It is inversely proportional to T_p.

$$V_{un} = \pm\frac{\lambda}{4T_p} \quad , \tag{2.7}$$

Maximum unambiguous range and unambiguous velocity are desired to be as large as possible. However, conflicting dependence of both parameters on T_p creates the well-known radar dilemma where increasing V_{un} decreases R_{un} and vice versa. This is an important consideration in radar design.

2.3 Simple Radar Equation and Signal Model

The radar equation relates the received power from a target to various radar and target parameters. The WSR-88D uses a parabolic dish antenna so all equations are developed for that antenna type. For a single target at radar boresight, Received Power P_r is expressed as

$$P_r = \frac{P_t G^2 \lambda^2 L}{(4\pi)^3 R^4} \sigma \quad , \tag{2.8}$$

(Skolnik, 2001), (Probert-Jones, 1962), (Doviak & Zrnic, 1993), (Battan, 1973)

where P_t is the average transmit Power,

G is the gain of the antenna,

L is the loss factor,

σ is the radar cross section of the target.

The loss factor L includes the effect of wave guide losses, antenna inefficiencies, beam attenuation, receiver bandwidth limitations and other factors. For a dish antenna, G is approximately

$$G = \frac{\pi^2}{\theta^2} \quad , \tag{2.9}$$

where θ is the beamwidth.

The radar equation (2.8) depends on scatterers in the far field of the antenna, defined at $\frac{2D_a^2}{\lambda}$ where D_a is the antenna's diameter (the far field is 1445m for the WSR-88D). From this point, the beam takes the idealized conical shape.

The radar signal power attenuates as it propagates through space. As such received signal is much weaker than the transmit signal. The ratio of the amplitude of the transmitted to received signal, α is given as

$$\alpha = \sqrt{\frac{P_r}{P_t}} \quad , \tag{2.10}$$

Weather radars transmits a pulse with In-phase (I) and Quadrature (Q) components. The transmitted pulse $x(f,t)$ of width τ can be expressed as

$$x(f,t) = A(t)\exp\left(j\left(2\pi f_t t + \theta(t)\right)\right) rect\left(\frac{t}{\tau}\right) \quad , \tag{2.11}$$

where $A(t)$ is the amplitude of the wave,

f_t is the carrier frequency,

$\theta(t)$ is the transmitter phase,

In-phase component is $I(f,t) = A(t)\cos\left(2\pi f_t t + \theta(t)\right) rect\left(\frac{t}{\tau}\right)$,

Quadrature component is $Q(f,t) = A(t)\sin\left(2\pi f_t t + \theta(t)\right) rect\left(\frac{t}{\tau}\right)$.

Alternatively, equation (2.11) can be written as

$$x(f,t) = I(f,t) + j\,Q(f,t) \quad . \tag{2.12}$$

At the time of receive, transmitted pulse would be delayed by the round-trip time to the target $\left(\frac{2R}{c}\right)$, shifted in frequency (f_D) and attenuated in amplitude by α. The received signal is thus,

$$y(f,t) = \alpha\, A\left(t - \tfrac{2R}{c}\right) exp\left(j\left(2\pi(f_t + f_D)\left(t - \tfrac{2R}{c}\right) + \theta\left(t - \tfrac{2R}{c}\right)\right)\right) rect\left(\frac{\left(t - \frac{2R}{c}\right)}{\tau}\right). \quad (2.13)$$

The latter can be expressed in terms of the transmit waveform

$$y(f,t) = \alpha\, x\left(f_t + f_D, t - \tfrac{2r}{c}\right) \quad . \quad (2.14)$$

2.4 Weather Radar Equation

In the previous, section the simple radar equation for a point scatterer was introduced. However, in real world applications of weather radar, received power is from a resolution volume filled with many scatterers. It is thus necessary to develop the radar equation for these scatters. In this section the Weather radar equation for scattering from a resolution volume is presented as discussed in Martin (2003).

The beam width for common meteorological radars, (Doviak & Zrnic, 1993) is given by

$$\theta = \frac{1.27\lambda}{D_a} \quad . \quad (2.15)$$

The resolution volume is the smallest volume within which echoes from all contained scatterers are integrated. It is defined by the beam width and range resolution of the radar. NEXRAD uses a pencil beam. So, the resolution volume is a $\theta\ by\ \theta\ by\ \Delta R$ volume, approximated as

$$\Delta V = \pi \left(\frac{r\theta}{2}\right)^2 \frac{\Delta R}{2} \quad . \tag{2.16}$$

The resulting equation (Battan, 1973) for the received power is

$$P_r = \frac{P_t G^2 \lambda^2 \theta^2 \, \Delta R \, L \sum_i \sigma_i}{1024 \, (ln2) \, \pi^2 r^2 \Delta V} \quad , \tag{2.17}$$

where $\frac{\sum_i \sigma_i}{\Delta V}$ is the total radar cross section per unit resolution volume.

Meteorological radars are designed to observe water drops, which are much smaller than the radar wavelength. Rayleigh approximation for RCS is assumed to hold. Using equation (2.1), Reflectivity factor, Z is calculated as

$$Z = \frac{\sum_i D_i^6}{\Delta V} = \frac{\lambda^4}{\pi^5 |K|^2} \frac{\sum_i \sigma_{Ray}}{\Delta V} \quad . \tag{2.18}$$

This is different from reflectivity η, defined as

$$\eta = \frac{\sum_i \sigma_i}{\Delta V} \quad . \tag{2.19}$$

It is common for the reflectivity factor converted to decibels, dBZ to be referred to as "reflectivity" however they are different parameters. Also, for cases where target size exceed the Rayleigh limit, the Rayleigh approximation fails and calculated Z is just an effective value.

Substituting (2.18) into (2.17), yields

$$P_r = \frac{P_t G^2 \theta^2 L \, \Delta R \, \pi^3 |K|^2}{1024 \, (ln2) r^2 \lambda^2} Z \quad , \tag{2.20}$$

The total radar cross section of scatterers in a volume can be recovered by equating equation (2.20) and (2.8) given by

$$\sigma = \frac{\pi^6 |K|^2 r^2 \theta^2 \Delta R}{16\,(ln2)\lambda^4} Z = 80.6 \frac{r^2 \theta^2 \Delta R}{\lambda^4} Z \quad . \tag{2.21}$$

If the resolution volume contains a single target, then eq. (2.21) is just the RCS of that target. Substitution of equation (2.9) into (2.20) yields

$$P_r = \frac{P_t L\, \Delta R\, \pi^7 |K|^2}{1024 (ln2) r^2 \lambda^2 \theta^2} Z \quad , \tag{2.22}$$

Converting to conventional units and substituting in constants,

$$P_r = 1.299 \times 10^{-16} \frac{P_t L\, \Delta R}{r^2 \lambda^2 \theta^2} Z \quad , \tag{2.23}$$

where ΔR is in m,

r is in km,

λ is in cm,

θ is in degrees,

Z is in $\frac{mm^6}{m^3}$,

L is dimensionless loss factor.

P_r is usually expressed in dBm which is decibels of Power relative to 1 mW,

$$dBm = 10\, log \frac{P}{0.001} \quad .$$

Expressing (2.23) in dBm gives

$$P_r\,(dBm) = -128.9 + 10\,log\frac{P_t \Delta R}{\theta^2 \lambda^2} + dBZ - 20\log R - system\ losses, \quad (2.24)$$

where, dBZ is reflectivity in logarithmic scale,

Radar Constant $RC = 128.9 + 10\,log\frac{P_t\,\Delta R}{\theta^2 \lambda^2}$, is an offset for received power.

2.5 NEXRAD

NEXRAD is a network of 160 high-resolution S -band radars (the locations are shown in fig. 2.2) operated by the National Weather Service. It produces three base data moments (Reflectivity Z, Mean Radial Velocity V and Spectrum Width σ_v) and three dual polarization variables (differential reflectivity Z_{DR}, Correlation Coefficient ρ_{HV} and Differential Phase φ_{DP}). (U.S. Department of Commerce; National Oceanic and Atmospheric Administration, 2016)

Data are collected in two resolutions: standard or super resolution. In the standard resolution, azimuthal sampling is done every 1 degree for a total of 360 radials per elevation. The super resolution on the other hand, has azimuthal sampling every 0.5 degree (720 radials per elevation). The latter resolution is normally used for the lowest 2 or 3 elevation scans. Reflectivity data are collected up to a range of 460 km while Doppler and dual polarization data are collected up to a range of 300 km. Range resolution is 250m for both. (U.S. Department of Commerce; National Oceanic and Atmospheric Administration, 2016)

The WSR-88D also operates in different Pulse Repetition Time (PRT) modes. The split cut mode is used at low elevation angles. The radar completes two scans at the same elevation, one with a long PRT (Contiguous Surveillance) to retrieve the unambiguous power from which Reflectivity and all dual pol variables are estimated. The second scan uses a short PRT (Contiguous Doppler) and so has more pulses to estimate Velocity, Spectrum Width and Reflectivity. The Split cut mode provides good ground clutter suppression. Birds and insects are known to stay at lower altitudes, thus all the data analyzed are obtained from this low elevation mode

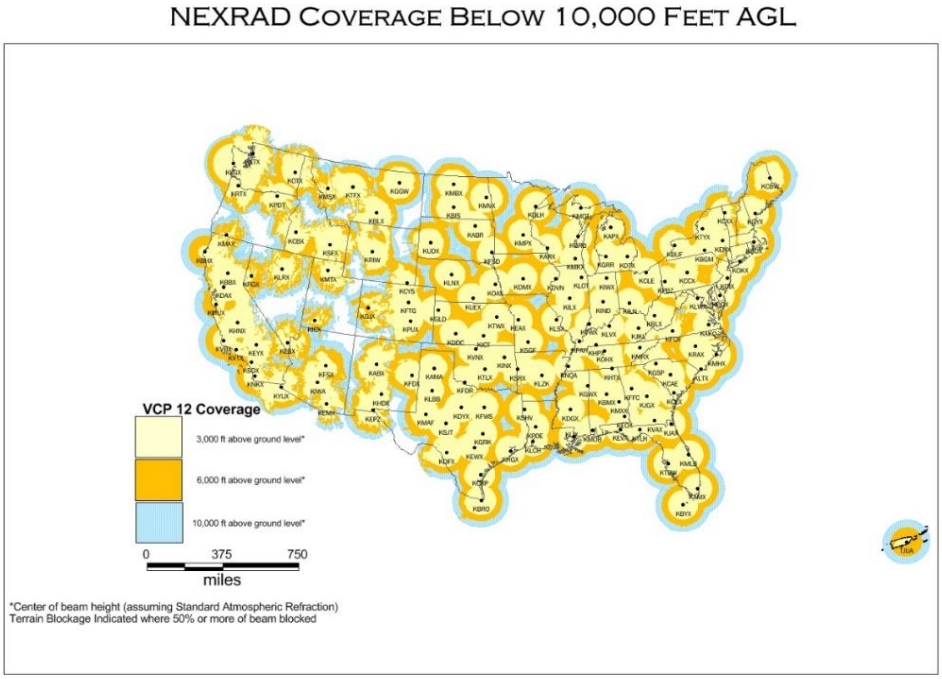

Fig. 2. 2 NEXRAD coverage of Contiguous US. Retrieved from (NOAA's National Weather Service Radar Operations Center, n.d.)

The Batch mode is used at intermediate elevation angles. The radar completes only one scan of interlaced long and short PRT's. The long PRT is used for unambiguous power while the short PRT is used to estimate range folded velocities. It has worse ground

clutter suppression than the surveillance and Doppler modes. At higher elevations, only the contiguous Doppler mode is used since range folding is not an issue.

Furthermore, NEXRAD switches between the clear air and precipitation operating modes chosen by comparing areas of observed reflectivity to a predefined threshold. Each mode contains different Volume Coverage Patterns (VCP) which are scanning strategies to maximize volume scanning. Precipitation mode has VCP's 11,12,21,121,211,212 and 221. Clear air mode has VCP 31 and 32. Each VCP contains a complete azimuthal scan at distinct elevation angles. Table 1 below shows the system specifications of the WSR-88D. It has an intrinsic beam width of 0.925° which means that the resolution volume has a $0.925° \times 0.925° \times 250\text{m}$,i.e., the elevation by azimuth by range volume. It is also highly sensitive being able to detect targets with an RCS 4 cm^2 (equivalent to a single bird) at 100 km.

Table 2. 1 Specifications of WSR-88 D

Transmitter	
Operating frequency	2.7 – 3 GHz
Wavelength	10.0 – 11.1 cm
Transmit power (peak)	700 kW
Polarization	Dual (simultaneous H and V transmit/receive)
Pulse width	1.57, 4.7 μs (235 – 705 m)
Antenna	
Diameter	8.5 m (parabolic dish)
3 dB beamwidth (at 2850 MHz)	0.925°
Gain (2850 MHz)	45.5 dB
First sidelobe	-29 dB
Maximum Rotation rate	30°/s
Receiver	
Minimum detectable signal, long pulse	-7.5 dBZ_e at 50 km
Minimum detectable signal, short pulse	-23.0 dBZ_e at 25 km
Gate Spacing	250 m
A/D convertor bits	16 bits
Point target detection	4 cm^2 at 100 km

(Palmer, et al., 2011) (Radar Operations Center, n.d.)

2.6 NEXRAD level II products

This section discusses the meaning and derivation of the 6 WSR-88D products. When a transmitted pulse scatters off targets in a resolution volume, total power at distinct doppler shifts (radial velocities) is reflected to the receiver. Doviak and Zrnic (1993) present the calculations of radar products elaborated below. The distribution of power as a function of doppler shift is called the doppler spectrum, $V(m, f_D)$. It is a function of pulse number m and doppler frequency f_D. Radar collects M samples of raw voltage: $V(0), V(1)$ $\ldots . V(M-1)$.

To derive radar variables, the autocorrelation of samples is calculated at lag 0, $\hat{R}(0)$ and lag T_p, $\hat{R}(T_p)$ as shown in (2.26) and (2.27) respectively. $\hat{R}(0)$ estimates the average power of a range gate.

$$\hat{R}(0) = \frac{1}{M}\sum_{m=0}^{M-1} |V(m)|^2 \quad , \tag{2.25}$$

$$\hat{R}(T_p) = \frac{1}{M-1}\sum_{M=0}^{M-1} V^*(m)V(m+T_p) \quad . \tag{2.26}$$

2.6.1 Reflectivity Z

Reflectivity measures the amount of power returned by a resolution volume in the horizontal channel. It provides information about the size or abundance of scatterers. Z is calculated as

$$S_H = \hat{R}(0) - N \quad ,$$

$$dBm = 10\log_{10}\left(\frac{S_H}{0.001}\right) \quad , \tag{2.27}$$

where S_H is the power returned in the H channel,

N is the noise power,

dBm is Power Received in decibels (dB).

Measured reflectivity is affected by many factors like the range r, radar specifications and system losses. Level 2 reflectivity presented for NEXRAD corrects for these factors. Thus, the final product is given as

$$dBZ = dBm + RC + 20\ log\ R + losses \quad . \tag{2.28}$$

2.6.2 Velocity V

The Doppler velocity is the power weighted average radial velocity of targets in a resolution volume. It is a projection of target velocities to the direction of the radar beam. When the target's velocity is approximately parallel to the radar beam, the magnitude of V is directly proportional to the targets speed. However, as the target's velocity approaches being perpendicular to the radar beam, magnitude of V approaches zero. Hence, low V might not always mean slow moving targets. For Weather Radars, negative values imply an approaching target while positive values represent a receding target. It is calculated from the H channel using a computationally efficient technique called pulse-pair processing given as

$$V = -\frac{\lambda}{4\pi T_p}\arg[R(T_p)] \quad . \tag{2.29}$$

2.6.3 Spectrum Width σ_v

Spectrum Width quantifies the variation of radial velocities in a resolution volume. Specifically, it is the consistency of phase change from pulse to pulse. High $\boldsymbol{\sigma_v}$ values imply variable phase change between pulses or a high diversity in the radial velocity of scatterers. $\boldsymbol{\sigma_v}$ is also calculated from the H channel as

$$\sigma_v = \frac{v_a\sqrt{2}}{\pi}\left|ln\left(\frac{R(0)-N}{R(1)}\right)\right|^{1/2} \quad . \tag{2.30}$$

2.6.4 Differential Reflectivity Z_{DR}

Differential Reflectivity is the difference between power returned between the vertical and horizontal channel. Z_{DR} gives information about the shape of scatterers in the resolution volume. For instance, Z_{DR} > 0 dB imply that scatterers have a larger horizontal cross section like an ellipsoid while Z_{DR} = 0 dB implies that they have a spherical shape. Negative values indicates scatterers that are more prolonged in the vertical direction. (Kumjian, 2013)

Z_{DR} is calculated as

$$Z_{DR} = dBZ_H - dBZ_v \; . \tag{2.31}$$

2.6.5 Differential Phase φ_{DP}

Differential phase, $\boldsymbol{\varphi_{DP}}$ is the propagation delay (or phase difference) between signals in the H and V channels (Kumjian, 2013). It provides information about water content and density of scatterers in the atmosphere. For example, a range gate that is densely

filled with precipitation will have a high $\boldsymbol{\varphi_{DP}}$ because the returned waves at H and V polarizations will be significantly delayed as they propagate through that gate. However, if the range gate is sparsely filled with precipitation, the wave will experience less resistance while propagating thus radar measures a lower $\boldsymbol{\varphi_{DP}}$.

The differential phase is calculated as the angle subtended by vector multiplication (cross correlation) of pulses in the H and V channels. Fig. 2.3 shows the calculation of $\boldsymbol{\varphi_{DP}}$ for three different pulses. For averaging several pulses, it is the angle subtended by the vector sum of the cross correlation.

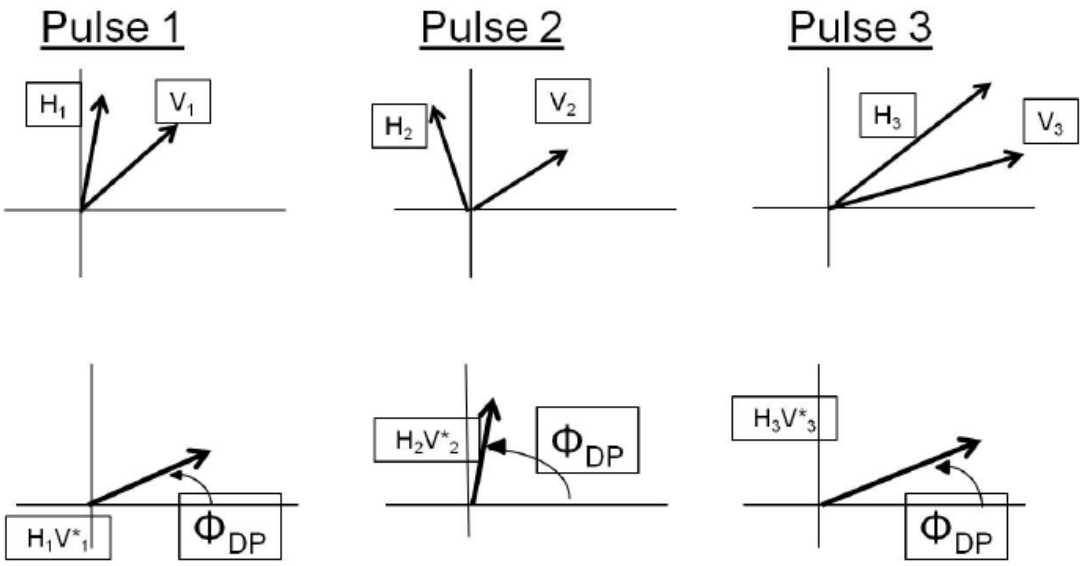

Fig. 2. 3 Calculation of φ_{DP} for three distinct pulses. Retrieved from (Dual-Polarization Radar Principles and Systems Operations, 2018)

2.6.6 Cross Correlation Coefficient $\boldsymbol{\rho_{HV}}$

$\boldsymbol{\rho_{HV}}$ measures the consistency of returned power and phase between both channels for each pulse. It is calculated as the cross correlation of pulses from H and V, normalized by the average power in both channels expressed as

$$\rho_{HV} = \frac{|\hat{R}_{HV}(0)|}{[S_H S_V]^{1/2}} \quad , \tag{2.32}$$

where $R_{HV}(0)$ is the cross correlation of H and V, given by

$$\widehat{R_{HV}}(0) = \frac{1}{M}\sum_{m=0}^{M-1} V_H^*(m)V_v(m) \quad . \tag{2.33}$$

$\boldsymbol{\rho_{HV}}$ values are usually between 0 (totally uncorrelated) and 1(totally correlated). Estimates of $\boldsymbol{\rho_{HV}} > 1$ are unreliable estimates. It gives information about the diversity of scatterers. This diversity includes properties like type, shape, orientation of particles or any feature that affects returned amplitude and phase (Kumjian, 2013). Precipitation such as pure rain has uniform shape and distribution and so have $\boldsymbol{\rho_{HV}}$ >0.97. Biological scatterers on the other hand are of varied sizes and exhibit distinct behavior. As such, they have a lower value, $\boldsymbol{\rho_{HV}} < 0.80$ (Park et al, 2008). Simply put, more coordinated scatterers have high $\boldsymbol{\rho_{HV}}$ and vice versa.

2.7 Clear Air Echoes

2.7.1 Nature/Origin of Clear Air Echoes

The origin of radar clear air return has been a subject of debate for a long time. Studies by Zrnic and Rhyzkov (1998) discovered that day time clear air returns had higher Z_{DR} and lower ϕ_{DP} than night time returns. They assumed that this was because insects were aloft in the day while birds flew in the night. While there was no independent data to confirm this conclusion, it is obvious that a change in scattering mechanism exists between day and night. In this thesis, clear air data is analyzed from September 2017, to explore the characteristics and origin of clear air return. The existing body of research has identified three main causes of clear air return: birds, insects and turbulent Bragg

scatter. Smoke and dust particles have been found to occasionally contribute to clear air return. However, they have a minimal effect because they are very small in size and occur too sparsely compared to birds/insects. Interference and solar radiation are also rare causes of clear air return.

Birds are large targets capable of independent flight with air speeds of 10-20 m/s (Martin, 2003). Their velocities pose an issue for radar derived wind estimation at night. The NOAA's wind profile routinely flags nocturnal clear air data as being contaminated by birds. A common feature of clear air data are angel echoes which are due to large targets. Ornithologists suggest that these angel echoes are caused by birds. (Eastwood, 1967), (Gauthreaux & Belser, 1998). Other studies by meteorologists (Zrnic & Ryzhkov, 1998; Jungbluth et al., 1995; O'Bannon, 1995) support bird contamination at X-band. Insects are smaller than birds and are generally wind borne except in cases of alignment where the aligned group generates its own velocity (Riley, 1975). As such they are good tracers of the wind. Insects can be found at any time of the day in large numbers and more uniformly spread in the atmosphere compared to birds.

Another accepted cause of clear air return is turbulent Bragg scatter. This occurs when turbulent flow mixes fluid across some refractive index gradient creating a field of refractivity perturbations which reflects radar signals. Kropfli et al. (1968), confirmed their presence with agreements between expected reflectivity and that measured with radars of different wavelengths. However, turbulent Bragg scatter is weak at S band (10 cm wavelength) leaving birds and insects as the main cause of clear air echoes in this study. Specular reflections off refraction gradients also cause clear air echoes for vertical pointing radars (Friend, 1939; Lane & Meadows, 1963) however S band

wavelengths are too short to cause such reflection. In the following sections, the characteristics of clear air echoes, birds as a cause of nocturnal echoes and insects as the cause of day time echoes are discussed in more detail.

2.7.2 Characteristics of Clear Air Echoes

Clear air reflectivity has a unique daily cycle. (Martin, 2003) analyzed clear air data collected from the Cimarron radar on the night of May 31, 1999. The results (in fig 2.4 below) showed that Z had stronger nocturnal return than day time return with the lowest values recorded at sunrise and sunset. During day time, Z maintained a modest value concentrated at a low height. This continued till sunset at 2 UTC where it reaches the first minima. In the next 1 hour, Z rapidly increases to its maximum value contained a greater height (2 - 3 km). The Average nocturnal value remains high between 4 – 10 UTC after which it rapidly drops to the second minima at sunrise (11 UTC) followed by a quick increase to around initial day time Z values. This cycle implies a clear change in nature (probably taxa) of scatterers between day and night. Hardy & Glover (1966) suggested daily cycle is due to insect of one specie leaving and another ascending. However, results from the analysis of dual pol variables in this research, show that the more plausible explanation is more insects flying during the day and birds dominating night returns. This is also supported by similar research reviewed.

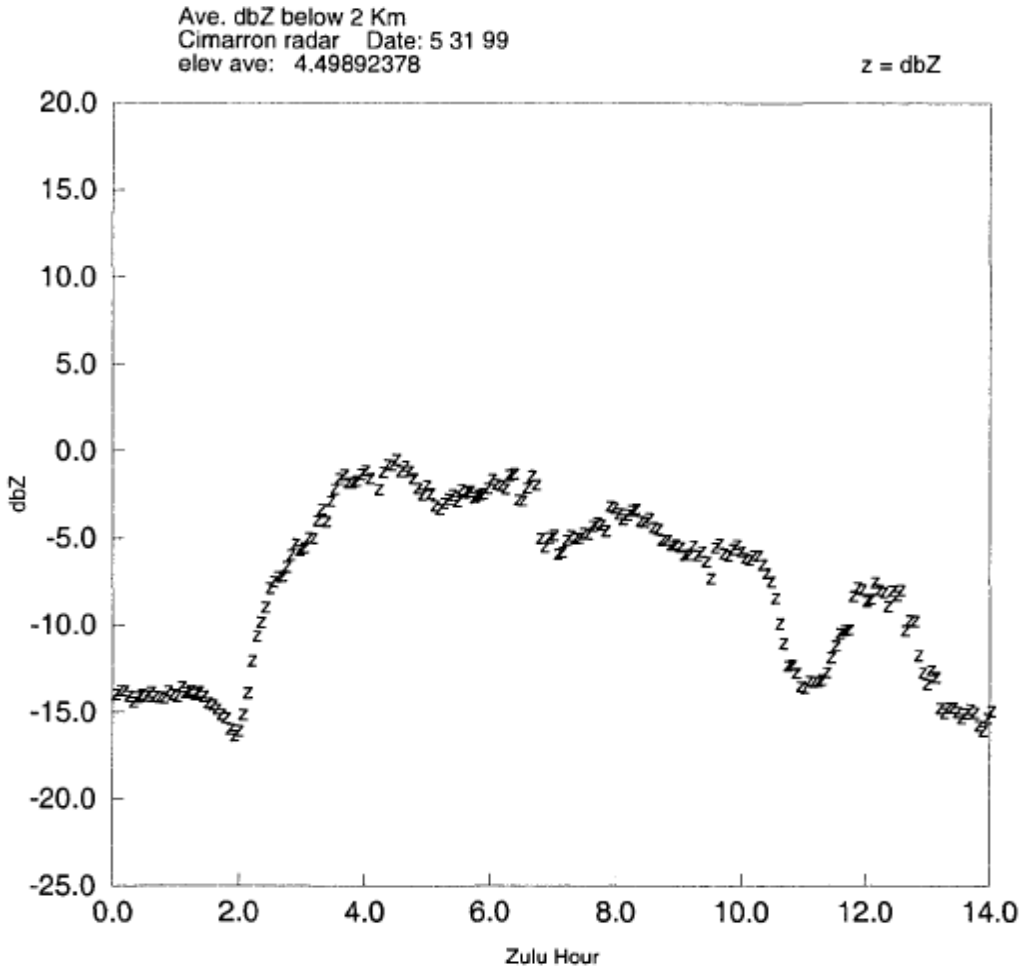

Fig. 2. 4 Average Reflectivity below 2 km versus time for a nocturnal case. Sunset is at 2Z and Sunrise is at 11Z. Data is from Cimarron radar collected May 31, 1999. (Martin, 2003)

Clear air echoes can occur as isolated targets and is often granular. Browning & Atlas (1966) discovered that nocturnal echoes have larger grains indicative of larger particulates compared to day time. This is probably due to more birds being aloft. Clear air echoes can also occur as layers or volumes filled with reflectivity (Martin, 2003). Furthermore, clear air Z fluctuates with seasons. Generally, it is stronger in the warm season. In the Great Plains, late spring has the strongest Z at night with daily values

fluctuating by as much as 20 dBZ (Martin, 2003). This correlates with the peak migrating season for birds.

Thin lines of clear air Z are a common feature of day echoes in the great plains. They are clearest (thinnest and sharpest) in the late afternoon. Wilson et al.(1994) attributed it to insects gathering at meteorological boundaries. Boundaries are also locations of large and sharp index of refraction gradients however, specular reflection is non-existent because at S-band because the radar wavelength is too short. Moreover, it is known that Convective Boundary layer marks regions with high insect abundance. Geerts & Miao (2005) studied vertical flight of scatterers in the Convective Boundary Layer using profiling air borne radar data collected during late spring in the great plains. They found insect plumes to be collocated with updrafts. Micro-insects were also observed to resist updraft with an average speed of 0.5 ± 0.2 m/s. They concluded that this fact explained the social behavior of small insects providing evidence of the biotic nature of insect plumes (thin line echoes).

Perhaps the strongest evidence of birds are the expanding rings of reflectivity often seen at certain morning times of the year. Elder (1957) initially postulated gravity waves as the cause. However, recent research has proven that it is due to birds leaving their nesting sites evidenced by these rings always emanating from the same location (Battan, 1973), (Eastwood, 1967), (Gauthreaux & Belser, 1998). Similar rings are seen in the evening due to bats leaving their roosting sites. Other rings of 1 to 3 km diameters, which do not expand, have also observed (Martin, 2003). They are attributed to convective cells. (Doviak & Zrnic, 1993).

PPI scans of Z for day and night show bilateral symmetry with the strongest values 180 degrees apart. This also extends to dual polarization variables (Zrnic & Ryzhkov, 1999). The symmetry is due to the radar cross section of a non-spherical object changing with the radar viewing angle. Scatterers are aligned in one direction so the radar samples distinct aspects as they approach, fly over and recede the radar location. Schaefer (1976) attributed it to birds aligned in one direction. Gauthreaux & Belser (1998) attributed it to aligned insects.

2.7.3 Nocturnal Clear Air Echoes

Migratory birds have been found to travel long distances mostly at night, sometimes in flocks but also individually. Thus, nocturnal echoes for bird migration season is dominated by birds. NOAA's Enviromental Technology Lab (ETL) considers this a severe problem and routinely the flag low level radar wind profiler data, collected at night during migration season as bird contaminated (van de Kamp, et al., 1997), (Miller, Barth, Smart, & Benjamin, 1997), (Wilczak, et al., 1995). This was further corroborated by differences in balloon sounding data and radar derived winds during certain periods of the year at night time and where birds are expected to migrate. O'Bannon (1995) and Gauthreaux et al.(1998b) report on this issue with the NEXRAD VAD wind profiles. Wilczak, et al. (1995) observed the same discrepancies with long wavelength wind profilers. The differences recorded were as large as 15 m/s which is consistent with the expected velocities for birds. Comparisons between VAD's and rawinsondes show similar errors as would be expected for bird contamination.

While many birds are expected in nocturnal echoes during a migration season, it does not exclude other sources like insects. Gossard & Strauch (1983) counted separate

echoes with a 1.5 m resolution FM-CW radar on a night in July in Nebraska. They found a density of 1 echo per 12 meter cube over a depth of 500m. Martin (2003) concluded that this density would imply about 46 billion members over the state of Oklahoma alone which certainly excludes birds as the only cause of nocturnal echoes. Furthermore, birds have been observed to have reflectivity in the range of 5 to 15 dBZ (Gauthreaux & Belser, 1998). One bird in a radar probe volume can account for 10 dBZ of echo (O'Bannon, 1995). Martin (2003) estimated that using a probe volume of 100-meter cube and 1 bird per volume over the state of Oklahoma through a depth of 3 km will require 500 million birds at the instant of a radar scan which is highly improbable. Other scatterers (probably insects) must be present in nocturnal echoes to explain this number.

2.7.4 Day Time Clear Air Echoes

Most day time echoes are caused by insects. They are usually spread over a wide area and more uniformly distributed than birds in the atmosphere. Crawford et al. (1949) concluded that insects are the cause of nearly all clear air echoes. This was based on the difficulty in creating gradients in refractive index strong enough to be sensed by the radar and visual confirmation of the presence of insects coinciding with radar observations.

Many other studies by entomologists have also confirmed insect dominance of day time clear air echoes. Drake (1984,1985) studied moths in Australia in a nocturnal low-level jet in Australia. He observed bilateral symmetry in Z due to alignment of scatterers using a 3.2 cm radar. Rapid increase in reflectivity at dusk was observed and attributed to mass insect takeoff. Aerial trappings with a kite borne net confirmed the presence of

moths up to 220 m. Drake (1984,1985) also reported radar cross section values of 1 cm^2 typical of large insects. These observations led to the belief that measured echoes were from insects.

Hardy & Katz (1969) compared clear air Z using radars with wavelengths of 3, 11 and 71 cm. They discovered that reflectivity of dot echoes in the lower troposphere decreased at higher wavelengths, consistent with Rayleigh scattering off objects smaller than radar wavelength. Wilson et al (1994) also used multiple radars with different wavelengths to study clear air echoes and concluded that insects were the cause of day echoes.

Kropfli (1986) used 3.22 cm and 0.86 cm radars to study the convective boundary layer during the day. They found difference between VAD winds and wind measured with a tall anemometer of about 0.2 m/s indicative of wind borne scatterers. Furthermore, typical clear air Z observed (-15 to 5 dBZ) where much higher than expected from the returns due to index of refraction gradients. They also noted an absence of maximum Z near inversion heights, ruling out refractive index gradients as the source. Based on these observations, Kropfli concluded that day clear air return was due to insects, seeds and particulates in the atmosphere.

Other studies by Hardy and Katz (1969) reported the presence of Bernard -like cells seen during the day at the same time an abnormal number of airborne ants were observed. However, it should be noted that birds can migrate any time of the year. Williams (2003) in his review of clear air echoes stated “Meteorologists should probably accept that it is possible for birds to be migrating at any time of the day or

night, on any day of the year, with any relationship to the weather and in any direction". Regularly observed birds flying in the atmosphere during day time easily confirms this assertion.

2.8 Classifying Birds vs Insects

Most studies by Meteorologists, Ornithologists and Entomologists use few variables to identify clear air echoes. However this approach will is error prone because NEXRAD variables are sensitive to target properties like location, range, aspect and radar cross section. For example, reflectivity depends on both radar cross section and abundance of scatterers in a range gate. Birds should generally have a higher average radar cross section. However, their backscatter cross section is in the resonance region. Some insects also have resonant cross sections. This means that a large insect observed broadside and a small bird observed head on can have similar cross sections. Thus, their respective Z values can be difficult to differentiate. Z also depends on the abundance of scatterers in the range gate. This means a strong Z echo can be due to a single bird, many insects, or a combination of both.

For a more robust classification, all other radar variables should be used . Birds are known to have higher velocities than insects. Consequently, radial velocities of birds will also be larger. Bachmann & Zrnic (2006) analysed the power spectrum of a resolution volume located in the direction wind was blowing. They found two peaks in the spectrum around 12 m/s and 20 m/s which they attributed to birds and insects respectively. Spectrum Velocity Azimuth Displays (SVAD) also showed insects with a Z_{DR} maximum between 3 and 8 dB while birds have a Z_{DR} < 2.5 dB. Insects generally have higher Z_{DR} than birds.

Furthermore, birds engage in more wind independent flight than insects. As such, resolution volumes dominated by birds would have a higher variation of radial velocities (or σ_V). Similarly, birds are less coordinated and uniformly distributed than insects when flying and should have a lower correlation between horizontal and vertical polarizations ρ_{HV}. Finally, birds have more liquid content than insects and so penetrating waves will be more delayed hence a greater phase change between H and V polarized waves. Birds should have higher ϕ_{DP} values than insects. Echoes assumed to be birds showed this behavior in the 1998 study by Zrnic and Rhyzkov.

More information can be derived from the level II products. A texture of these products is calculated as the spatial variability over a 3-range gate by 3-range gate contiguous volume (or texture volume) to obtain 6 products. They reveal patterns of clear air echoes that might exist over a larger spatial scale. For Example, Velocity texture shows uniformity of velocity over the texture volume. All 12 parameters are analyzed for consistency with the expected characteristics discussed above. The results are presented in greater detail in the next chapter. Obtained distributions are used in a fuzzy logic classifier to separate bird and insects echoes.

Chapter 3

Procedure

3.1 Data Collection

Radar data from KTLX WSR-88D radar (shown in fig 3.1 and 3.2) located in central Oklahoma was analyzed. Previous examination of radar data shows that reflectivity from birds and insects can have close values. Reflectivity of biota depends on volume density of species, so a high value of Z could mean a few large birds or many small insects. Therefore, a simple reflectivity threshold cannot be used alone to distinguish these scatterers. Other properties of the base data or/and dual – polarization (dual pol) radar parameters need to be utilized. The base data include Equivalent Reflectivity factor (hereafter Reflectivity) Z, Doppler velocity V and Spectrum Width σ_V. The dual polarization parameters are differential reflectivity Z_{DR}, differential phase φ_{DP} and correlation coefficient ρ_{HV} between the orthogonally polarized radar waves. The texture of a radar variable provides information about the variability of its spatial field over a certain volume, usually composed of several radar resolution volumes. The texture of each radar variable is also analyzed for potential information on separating echoes from birds and insects. More discussion on the texture is presented in section 3.2.2.

The algorithm will be applicable between 10 to 100 km from the radar. This is sufficient range for the terminal airport area, which typically has a radius of 50-70 km around the airport. Range gates that are located at less than 10 km from the radar are not considered because measurements are contaminated by ground clutter. Radar data show that all radar parameters vary with the distance from radar and azimuth of the radar

beam. Therefore, the algorithm can have variable parameters which can depend on the distance from radar. The following distance intervals are chosen for the algorithm: 10 – 20, 20 - 30, 30 – 40, 40 – 50, 50 - 60, 60 - 70, 70 - 80, 80 – 90, and 90 – 100 km. These are 9 range intervals. The radar parameters inside the intervals will be averaged to reduce natural fluctuations of the radar estimates.

3.1.1 Selection of Clear Air Days

The main goal of this study is designing an algorithm which classifies radar echoes from insects and birds. To obtain radar parameters for the algorithm and to tune it, cases with dominant reflections from insects and birds are needed.

It is known that September is a month with intense nocturnal bird migration in Oklahoma, so it is chosen in this study as the bird migration case. Clear air days, i.e days without precipitation were selected according to the mesonet data (shown in the top panel of fig 3.3) obtained from the Norman station. The rainfall rate is in inches. All days with rainfall less than 0.1 inches are selected. They are September 1,3-16 & 19 -25 all in 2017. This is a total of 22 clear air days.



Fig. 3. 1 Street View of KTLX WSR-88D radar



Fig. 3. 2 Satellite View of KTLX radar

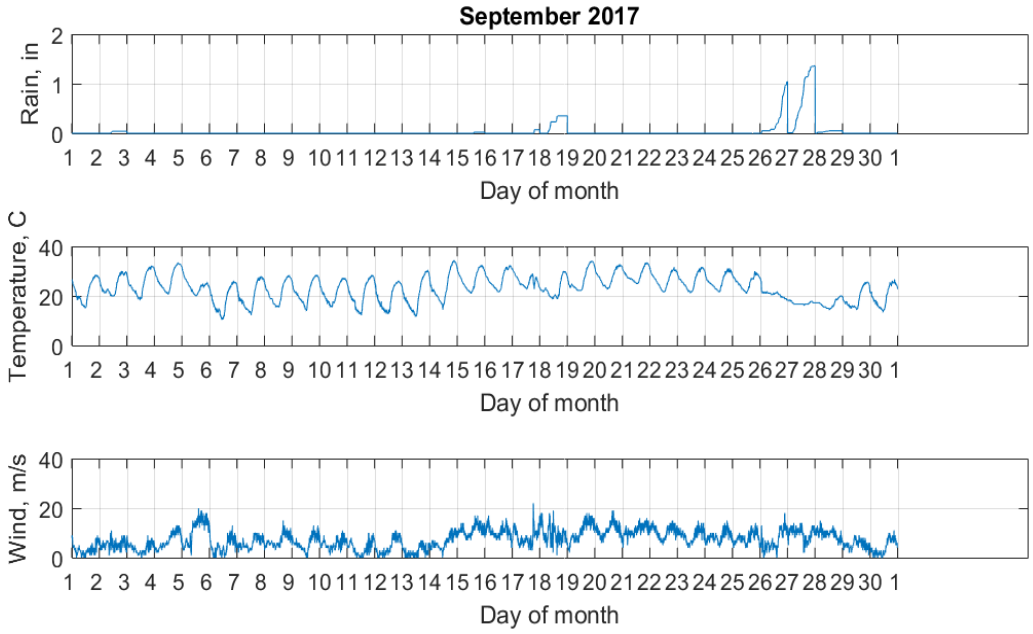

Fig. 3. 3 Mesonet Sounding for September 2017

3.1.2 KTLX Collection Mode

Data collection is done in two resolutions: standard and super resolution. In standard resolution, azimuthal sampling is done every 1 azimuthal degree for a total of 360 radials per elevation. For Super resolution on the other hand, azimuthal sampling is done every 0.5 degree (720 radials per elevation). It is normally used for the lowest 2 or 3 elevation scans. KTLX switches between clear air and precipitation operating modes: these modes are chosen by comparing areas of currently measured reflectivity to a predefined area threshold. Each mode contains different Volume Coverage Patterns (VCP) to maximize volume coverage. Clear air mode utilizes VCP's 31 and 32.

Data were combined from the two lowest elevation sweeps. The lowest elevation (Surveillance sweep) contains all dual polarization variables and Z for ranges

up to 460 km while the next elevation sweep (Doppler) contains Z, V and σ_V. Since both cuts are separated by less than a minute, they are considered as one sweep with dual pol variables estimated from the Surveillance sweep, and Z, V and σ_V estimated from the Doppler sweep. Z estimate from the Doppler sweep is chosen because it uses more pulses which translates to higher accuracy while maintaining a maximum unambiguous range of 148 km. This range is sufficient for the requirements of this study. Figure 3-4 shows example radar variables for the clear air scans, 4 Sept, 2017 at 20:00 UTC and midnight on 5 Sept, 2017. In raster scan order, the variables in fig. 3-4 are $Z, V, \sigma_V, ZDR, \varphi_{DP}$ and ρ_{HV}.

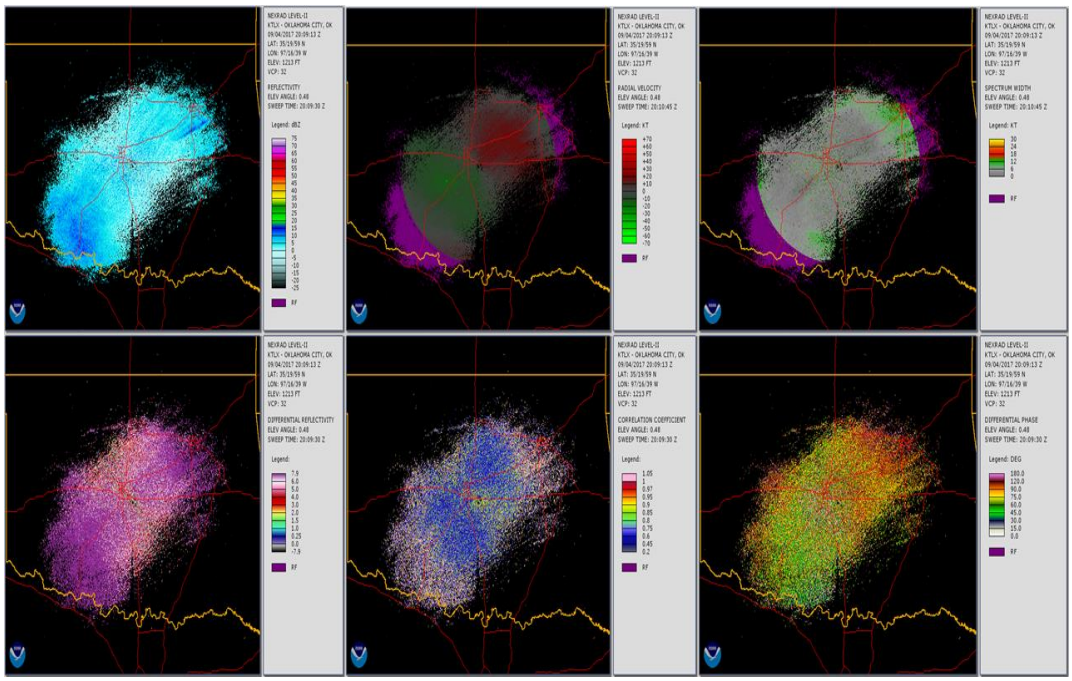

Fig. 3. 4 PPI plots showing data from Day Time (20:00 UTC). WSR-88 D KTLX, 4 Sept, 2017

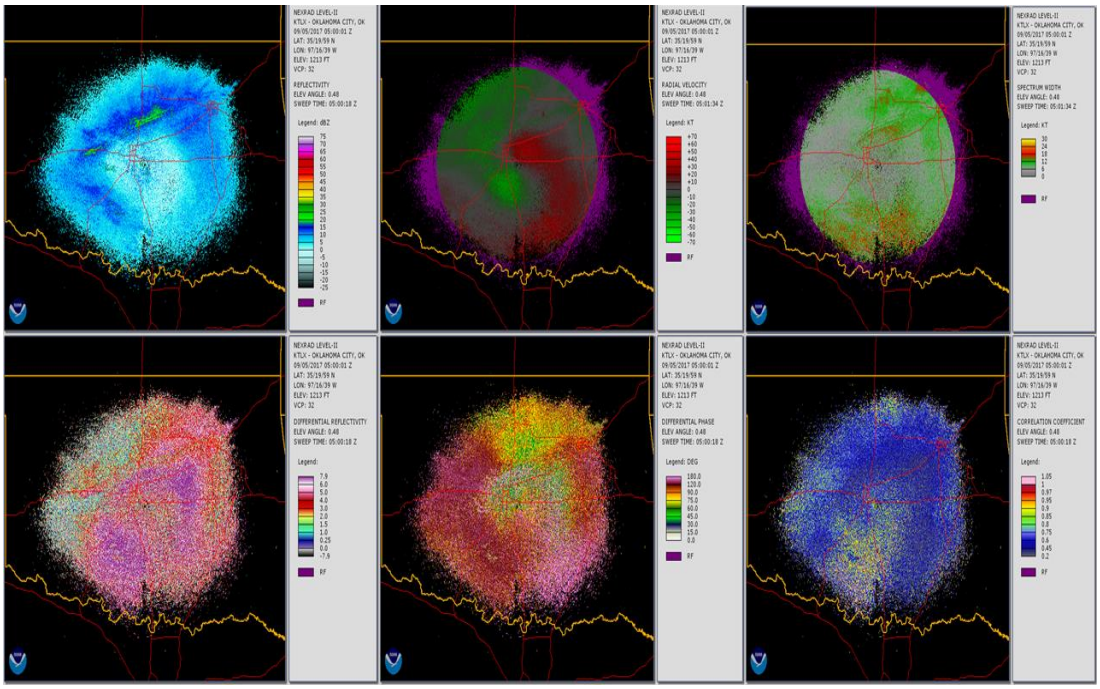

Fig. 3. 5 Same as fig 3.4 but for Midnight 5th Sept, 2017

3.2 Data Processing

The next step is processing the data to obtain distributions of radar parameters for birds and insects. Previous studies have shown that during migratory season, birds dominate night time clear air echoes while insects dominate day time clear air echoes. In this study, day time is defined as 14 - 21 UTC (9 – 16 CDT) while night time is defined as 2 - 9 UTC (21 – 4 CDT). A general overview of the data processing algorithm is shown in fig. 3.6. For day (night) time, the first step is to load data from all Plan Position Indicators (PPIs). Next, data quality control (or data preprocessing) is applied to remove data points that have either a low Signal to Noise Ratio (SNR), no measured values, precipitation or ground clutter. The third step is to calculate the texture of all radar variables. In the final data processing step, radar data is averaged first over 10 km along the radials and then each 10 km pixel is averaged over 30 minutes. The result of this step is 6 Median of Median Textures (MOM) and 6 Mean of Mean (MM) variables, totaling 12 parameters. Sections 3.2.1 – 3.2.3 presents more detail on data quality control, texture and data processing.

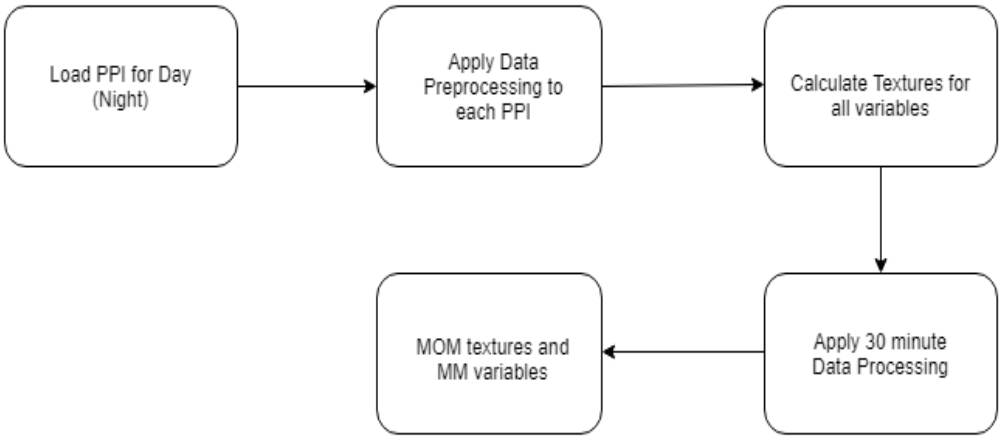

Fig. 3. 6 Flow chart of the data processing algorithm

3.2.1 Data Quality Control

Data were analyzed in 10 km intervals from 10-100 km. KTLX data is level II, so low SNR range gates and gates with anomalous propagation have been filtered out. The following thresholds are also applied

a) Data cells with -888 or -999 (low SNR) values were removed

b) Biological scatterers typically have low ρ_{HV} values with an upper limit of about 0.8 while precipitation have ρ_{HV} > 0.97 (Park et al., 2008). A threshold of $\rho_{HV} = 0.8$ has been chosen for this study to remove possible weather contamination while retaining biological echoes. All range gates with ρ_{HV} greater than this threshold are removed

c) All range gates with radial velocities in the range [-1,1] m/s are also excluded to prevent possible contamination by clutter.

3.2.2 Texture

Texture provides information about the spatial variability of a radar variable over a texture volume made up of neighboring radar resolution volumes. The texture volume used is a 3 by 3 contiguous grouping of gates centered on a reference gate. Each resolution volume is $0.925° \times 0.925° \times 250\text{m}$. Thus, the texture volume is $2.78° \times 0.93° \times 750m$. Fig 3.7 shows a texture volume made up of gates 0-9 and centered at reference gate 0. Gates 3, 4 & 5 belong to one radial, 1, 8 &7 to another and 2, 0 & 6 to the third radial. Rmin and Rmax are the lower and upper boundaries for a specified range interval. So, for a 10-20 km interval, Rmin = 10 km, and Rmax = 20 km.

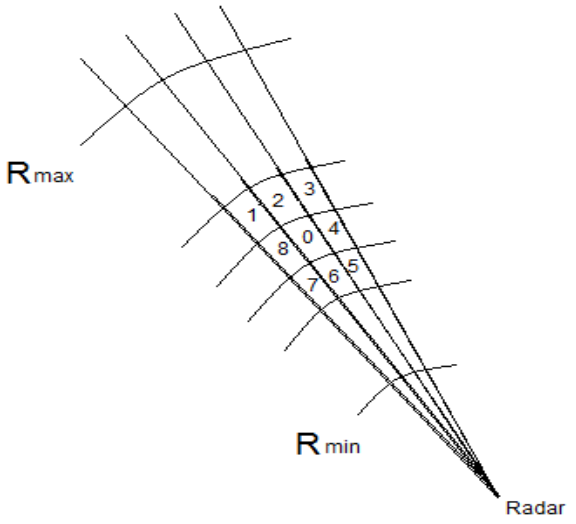

Fig. 3. 7 Set-up for calculating texture at gate 0

For Reflectivity Z, the texture $\Delta Z_{a,b}$ at radial a and range gate b is calculated as

$$\Delta Z_{a,b} = \frac{1}{N-1}\sum_{i=-1}^{1}\sum_{j=-1}^{1}\left|z_{a,b-} z_{a+i,b+j}\right| \quad (3.1)$$

where *i* the azimuthal offset and *j* is the range gate offset from the reference gate. N is the number of gates with measured values. Texture is only calculated if $z_{a,b} \neq NaN$ and $5 < N \leq 9$ .Otherwise the texture is assigned as not available (NA). This condition ensures that the texture is always representative of at least half of the texture volume. Edge effects for the first/last radials and range gates are handled by periodic extension. Also, ΔZ and ΔZ_{DR} are calculated using the values in dB (not linear scale). The same procedure is used to obtain texture for velocity (ΔV), spectrum width ($\Delta\sigma_V$), differential reflectivity (ΔZ_{DR}), differential phase ($\Delta\varphi_{DP}$), and correlation coefficient ($\Delta\rho_{HV}$).

3.2.3 Thirty Minute Data Processing

Data processing takes into consideration range, time and azimuthal dependence of radar variables. Data is processed along each radial, in 10 km range intervals It is also processed in 30-minute (half hour) intervals. Thus, for a radial at 20°, a half hour interval of 01:00-01:30 UTC and range interval 10-20 km, the procedures are

a) The texture of each variable is found using equation (3.1) for each Plan Position Indicator (PPI).
b) Median of texture along the 20° radial and between 10 – 20 km interval is found
c) All median textures in step b) is compiled for all PPI's within 01:00-01:30 UTC.
d) The median is found for the compiled textures in c). This statistic will be called the median of median (MOM) texture.
e) Repeat a) to d) for all radials, range intervals and time intervals.

A similar procedure is used to analyze the original level II variables the only difference being that mean is used instead of the median, and step a) is omitted. The resulting statistic will be called the mean of mean (MM) variables

3.3 Results

This section presents the distributions of radar parameters for night and day echoes. Each data point denotes a MOM texture or MM variable. The blue histograms represent data from night echoes while the red represents data from day echoes. All 12 parameters are compared to determine which ones show good enough separation between the two taxa. Hereafter in this report, day time is assumed to be the distribution of insects while night time is assumed for birds. Further discussion on each parameter is presented below.

3.3.1 Reflectivity Z

Reflectivity shown in fig.3.8 has a higher median for night time for all range intervals. This is expected because at night many birds are aloft is the atmosphere. Since they are bigger than insects and quite dense, they would have higher returned power. This parameter has very good separation between distributions for bird and insect echoes.

3.3.2 Velocity V

Birds are active fliers and would produce higher velocities than insects which are wind borne. This can be seen in fig 3.9 with night velocity between ± 25 m/s while day velocities are between ± 20 m/s. The wind velocity can change during a day and the Doppler velocity depends on wind velocity. The Doppler velocity also depends on the flight direction of birds/insects and is a projection of their true velocity unto the

direction of the radar beam. As a result, the distributions can be seen to be poorly separated.

3.3.3 Spectrum Width σ_V

Spectrum width measure the variation of velocities within the resolution volume. Bird occupied volumes will have a wider range of velocities compared to insect occupied volumes because birds are more active fliers than insects. Thus, the spectrum width for birds will be higher. This can be seen in fig 3.10 where birds have a higher median σ_V than insects across all ranges. Both distributions are also well separated.

3.3.4 Differential Reflectivity Z_{DR}

Studies by Zrnic and Rhyzkov (1998) observed insects to have high Z_{DR} (up to 10 dB) compared to birds. This can be seen in fig 3.11 where insect distributions have higher values across all ranges. Also, From 30 – 100 km, many insect values accumulate around 8 dB because this is the highest Z_{DR} that WSR-88 D can measure. Actual values are $\geq$ 8 dB, consistent with the previously mentioned studies. Both distributions are also well separated.

3.3.5 Differential Phase φ_{DP}

Zrnic and Rhyzkov (1998) also found that birds had higher φ_{DP}, sometimes exceeding 100° compared to insects. Median values for bird φ_{DP} (seen in fig 3.12) can be seen to be $\geq$ 100° and are also greater than median value for insects across all ranges. Furthermore, φ_{DP} shows very good separation for birds and insects.

3.3.6 Correlation Coefficient ρ_{HV}

Birds are large targets compared to radar wavelength, move in a less coordinated manner and are less uniformly distributed than insects . They will have a lower correlation coefficient compared to insects. This can be observed in fig 3.13 where insects have a higher ρ_{HV} for all ranges. Even though separation between birds/insects is not very large, it is consistent. Thus the distributions are considered to be well separated.

3.3.7 Velocity Texture ΔV

Velocity texture gives information about the variation of the mean Doppler velocity within texture volumes. Bird flight is less wind dependent than insects, so it is expected that this variation is higher for bird dominated echoes. It can be seen in fig.3.14 below that median bird ΔV is higher than that of insects for all ranges. ΔV is chosen for use in the algorithm instead of V because it is calculated by comparing V from three consecutive radials. Thus, the variation in V due to projection of actual target velocities to the radar beam direction and change in wind velocity is minimized. Distributions for ΔV are well separated.

3.3.8 Spectrum Width Texture $\Delta\sigma_W$

The separation between birds/insects for $\Delta\sigma_W$ (in fig 3.15) is not obvious from 10-50 km. However, at 50-100 km from the radar birds can be seen to have higher $\Delta\sigma_W$. The latter is consistent with the expectation that birds will have a larger variation in velocities. Overall, both distributions show good separation.

3.3.9 Other texture parameters

Fig. 3.16 shows the distribution of ΔZ. This parameter could in theory explain observed features of clear air Z such as granularity or volume filling. For 10 – 50 km, insects have slightly higher median values than birds. However, for other ranges, the separation between the two is not clear. Figs 3.17 – 3.19 also shows the distribution for texture of Z, Z_{DR}, φ_{DP} and ρ_{HV}. They all have similar modes in their distribution for birds and insects thus they are poorly separated.

In summary, Z, σ_V, Z_{DR}, φ_{DP}, ρ_{HV}, ΔV and $\Delta\sigma_W$ (7 parameters) shown in figs 3.8, 3.10 – 3.15 all show good separation between distributions for birds and insects for most range intervals. Furthermore, observed features of these parameters are consistent with day echoes being insects and night echoes being birds. However, V, ΔZ, ΔZDR, $\Delta\Phi_{DP}$ and $\Delta\rho_{HV}$ (5 parameters) shown in figs 3.9, 3.16 – 3.19 did not show clear separation.

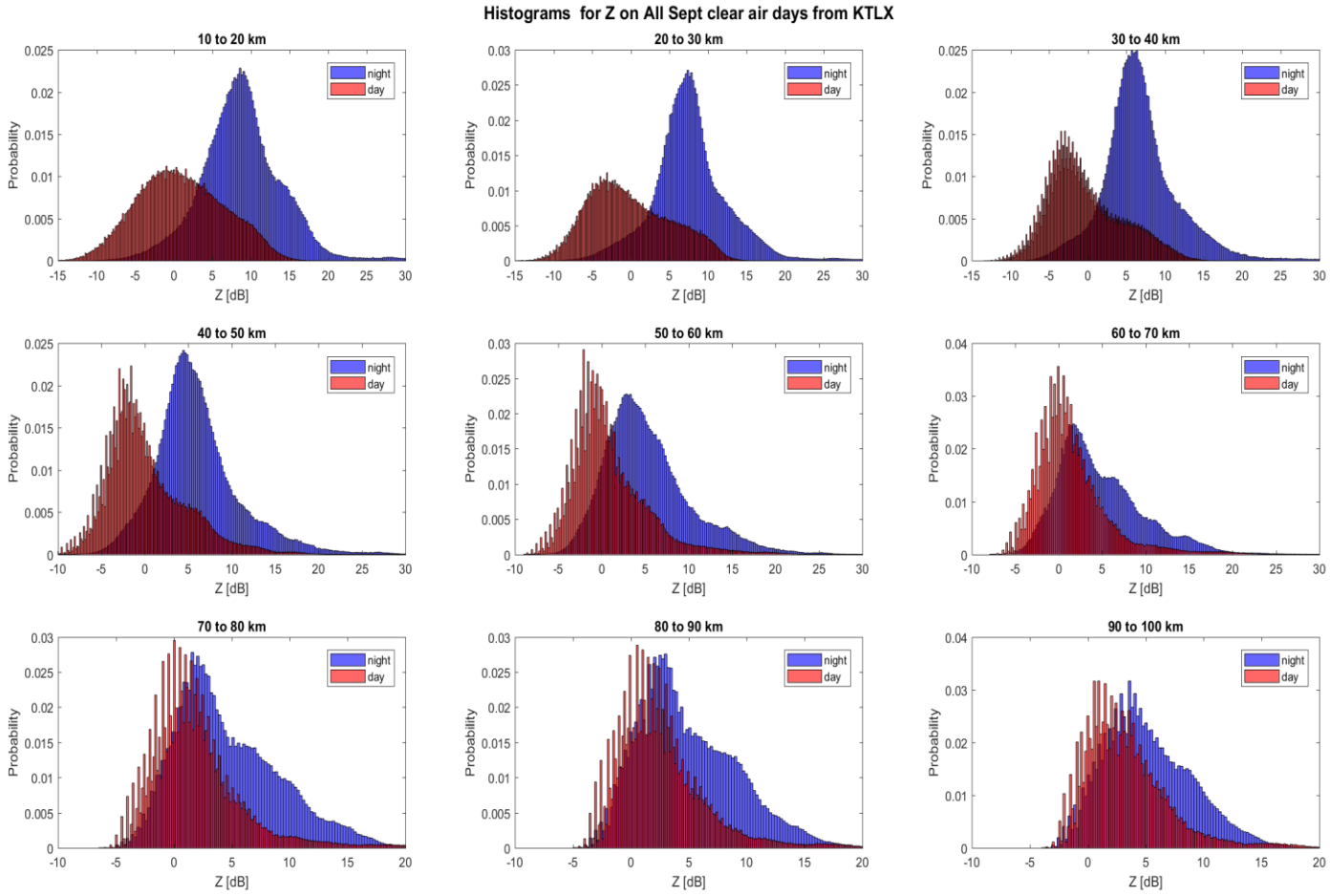

Fig. 3. 8 Distribution of Z for clear air days in September 2017.

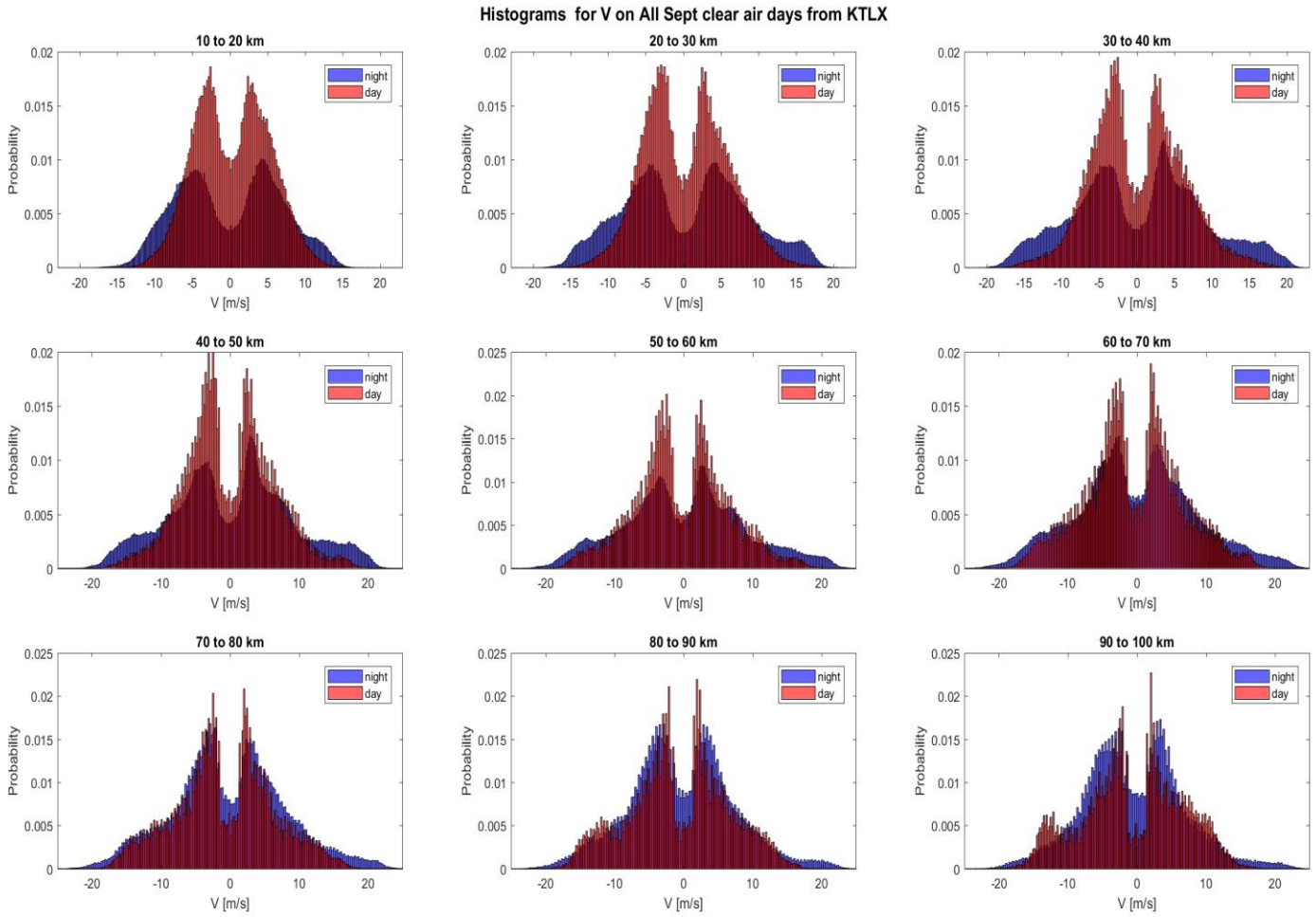

Fig. 3. 9 Same as 3.8 but for V

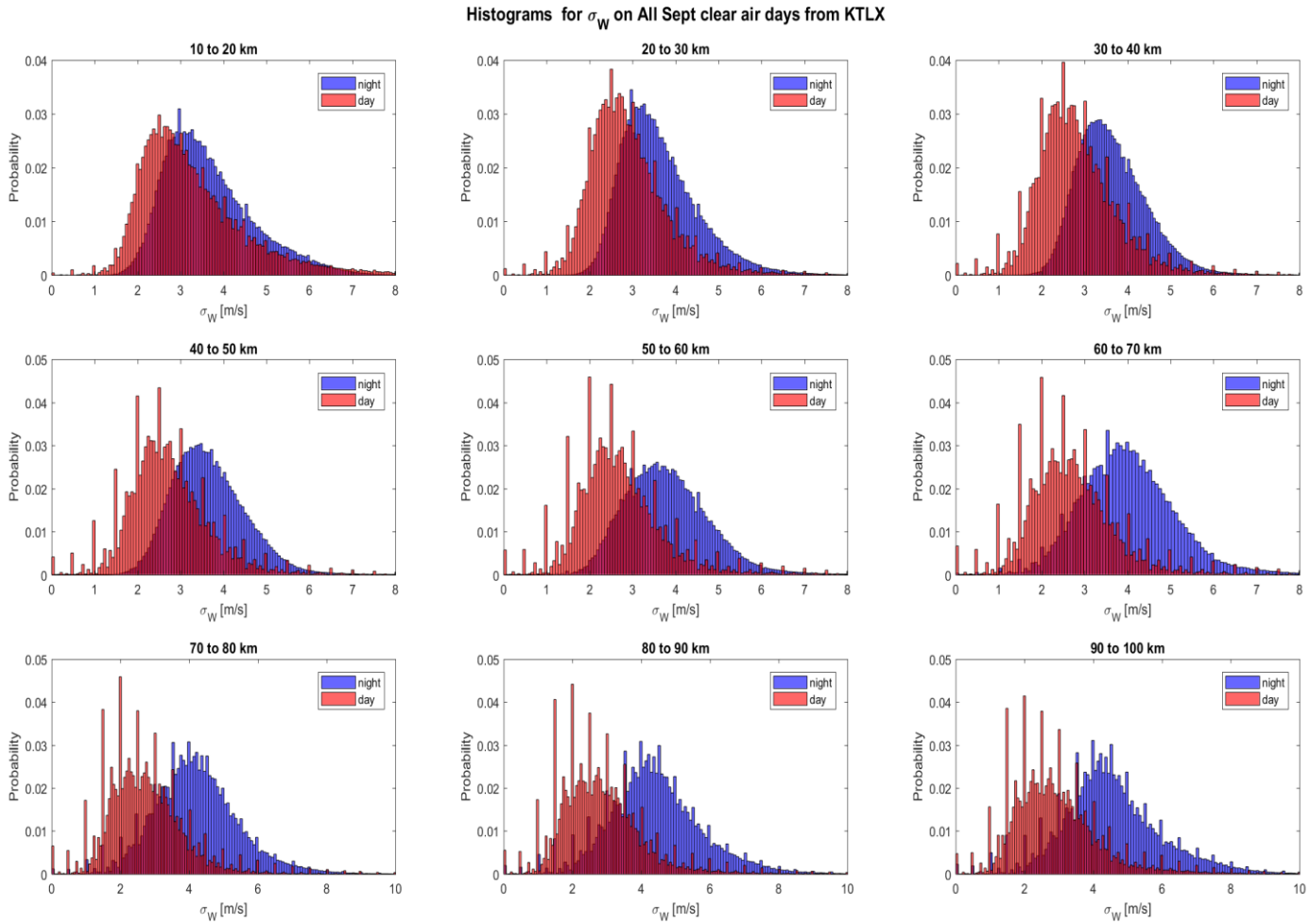

Fig. 3. 10 Distribution of σ_V for clear air days in September 2017

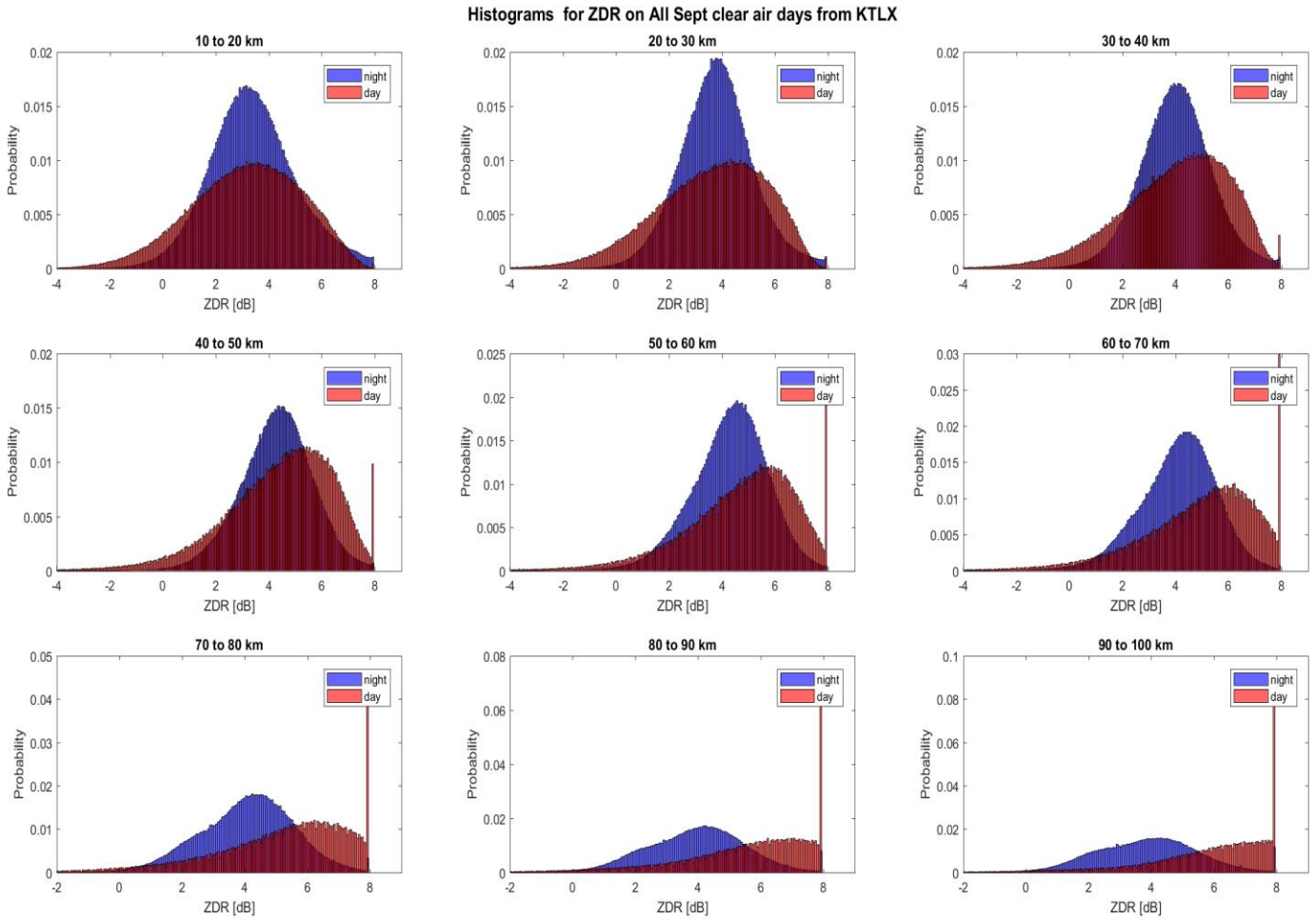

Fig. 3. 11 Distribution of Z_{DR} for Clear Air Days in September 2017

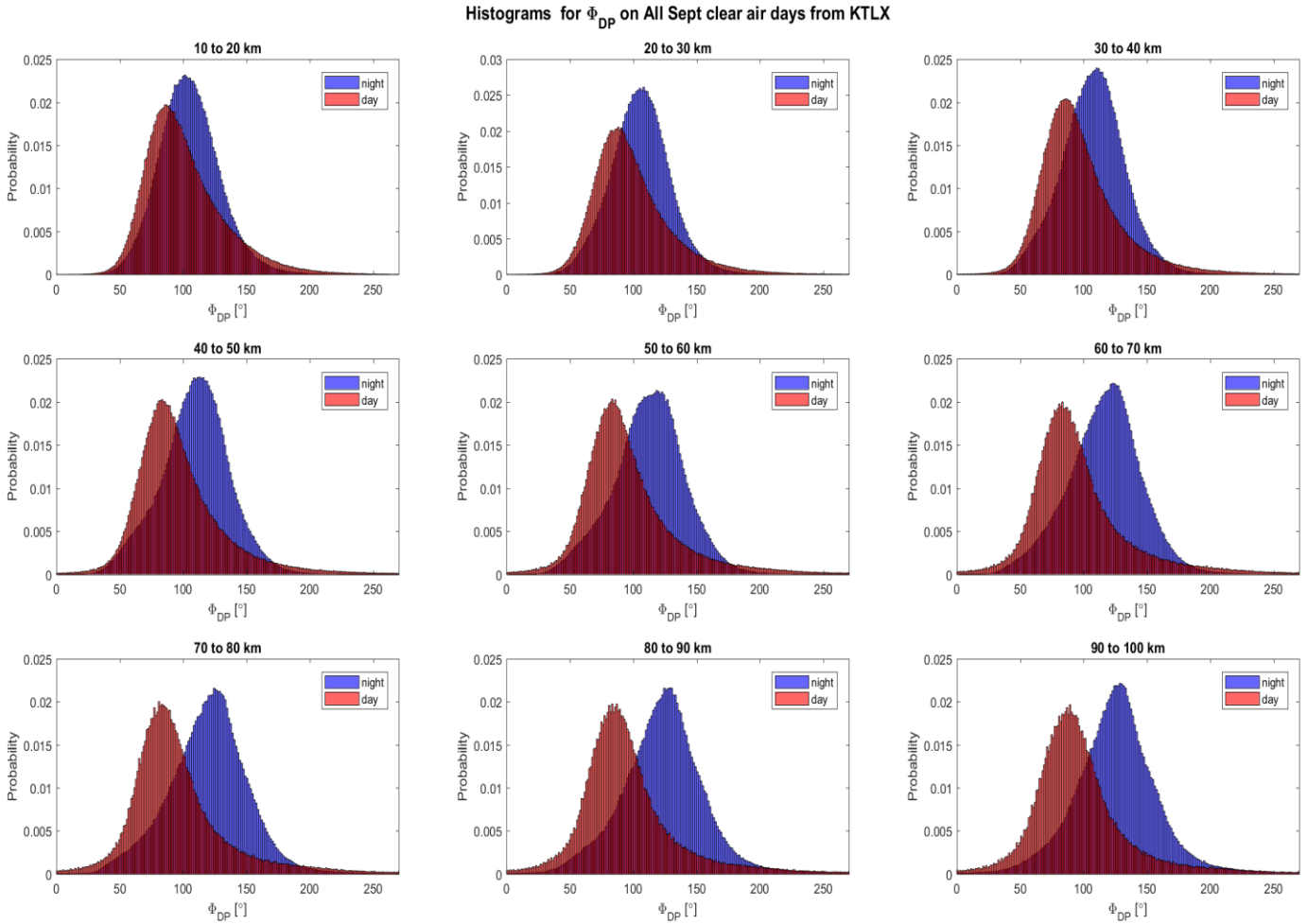

Fig. 3. 12 Distribution of φ_{DP} for clear air days in September 2017

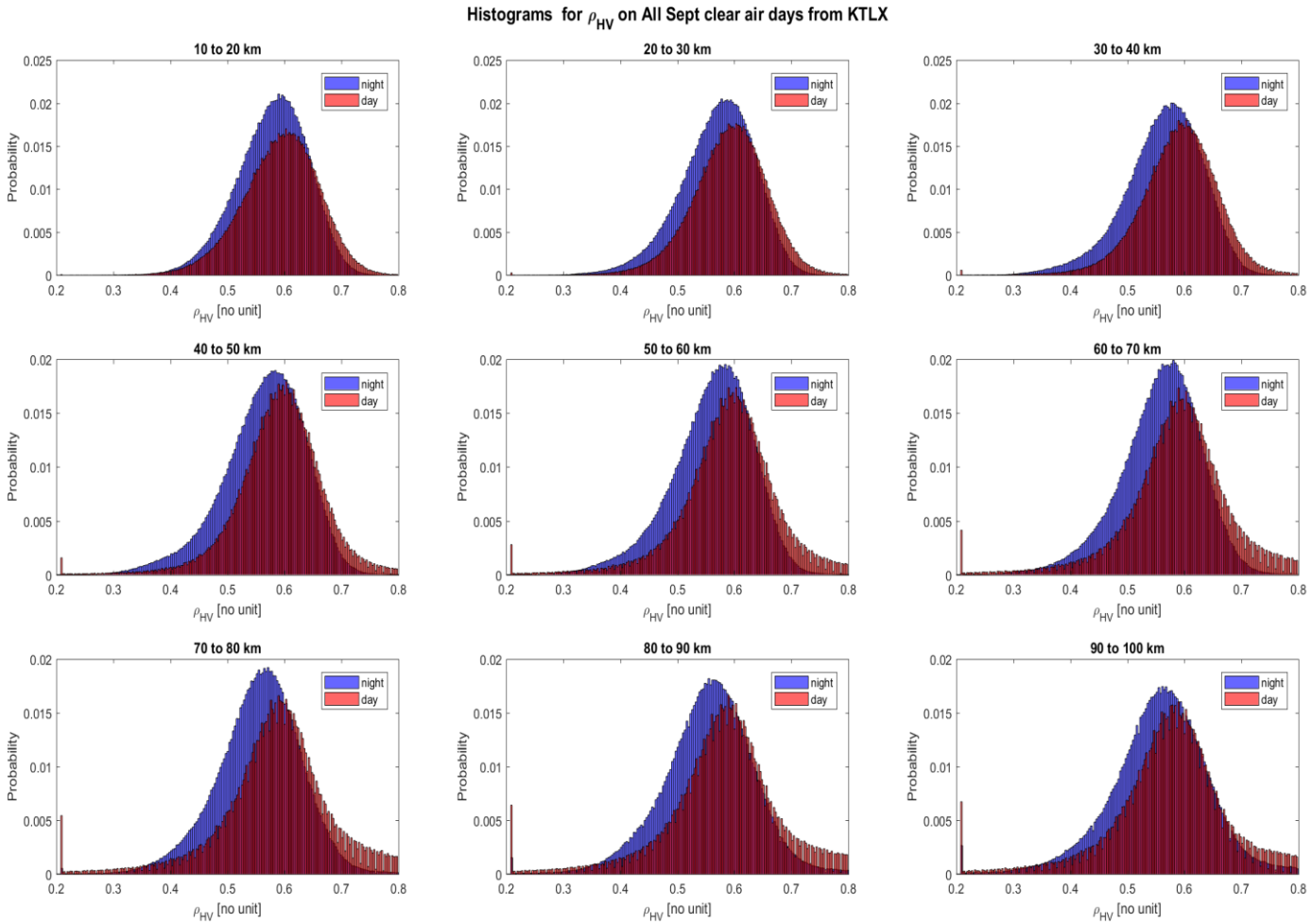

Fig. 3. 13 Distribution of ρ_{HV} for clear air days in September 2017

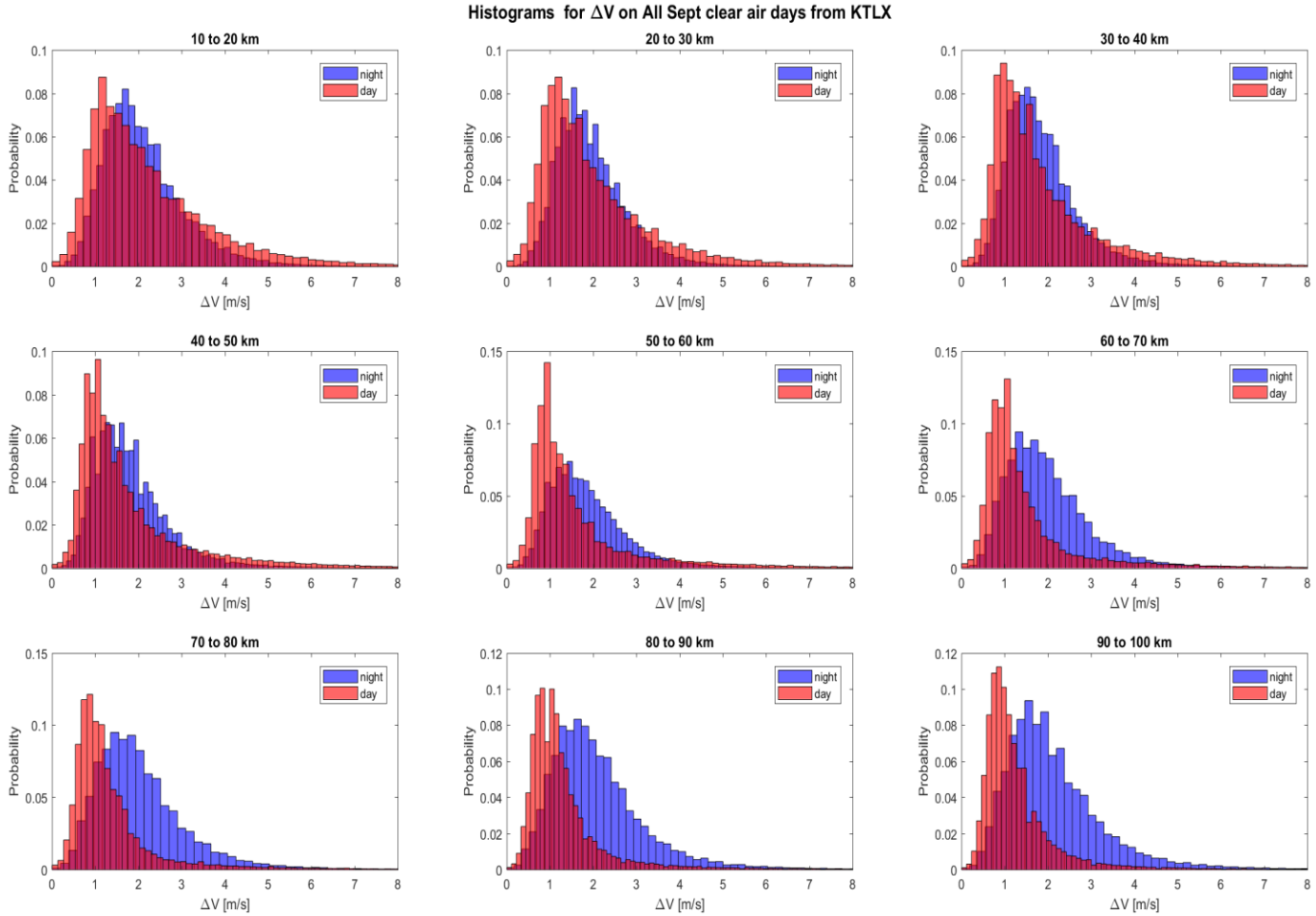

Fig. 3. 14 Velocity texture ΔV

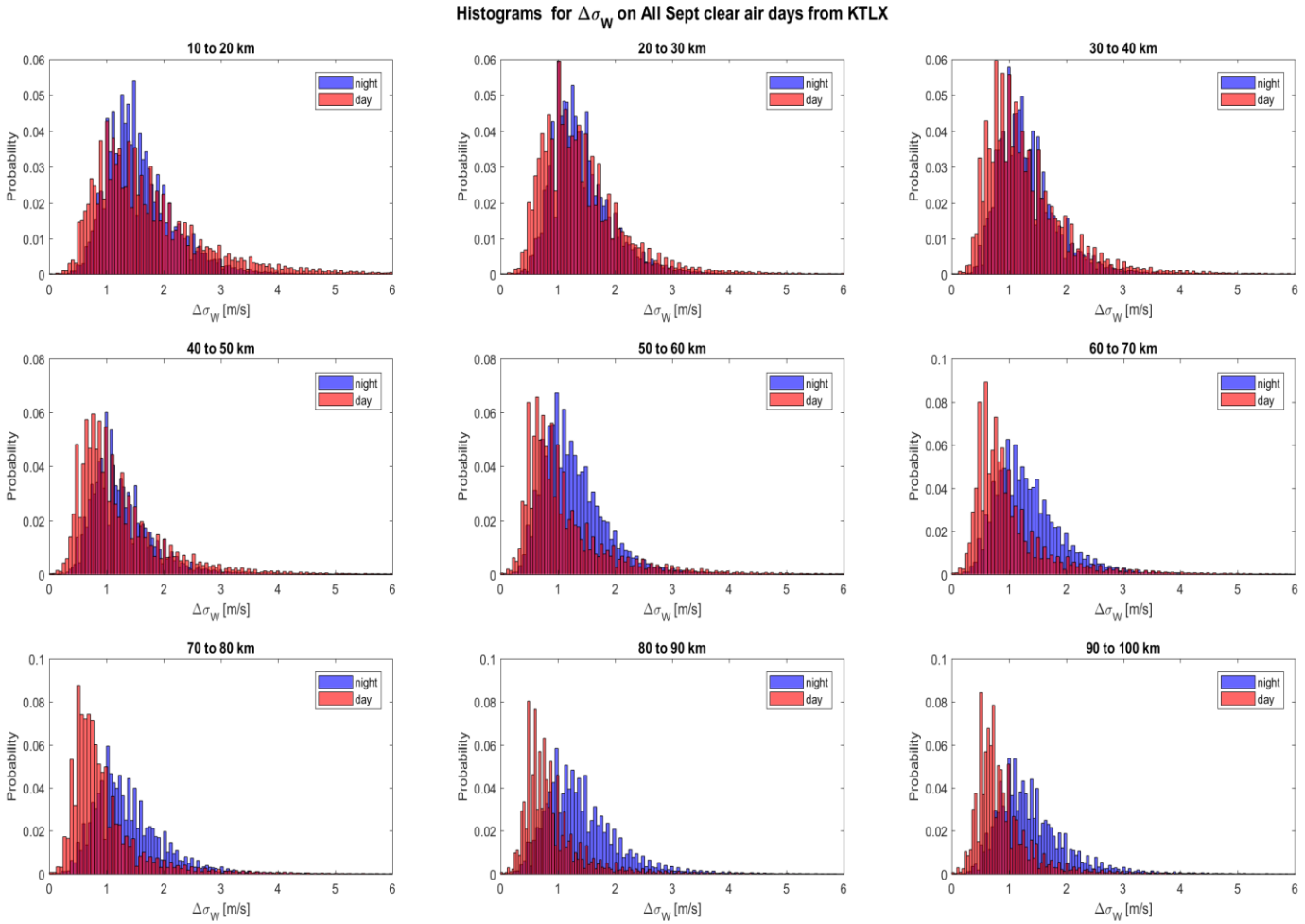

Fig. 3. 15 Spectrum width texture $\Delta\sigma_V$

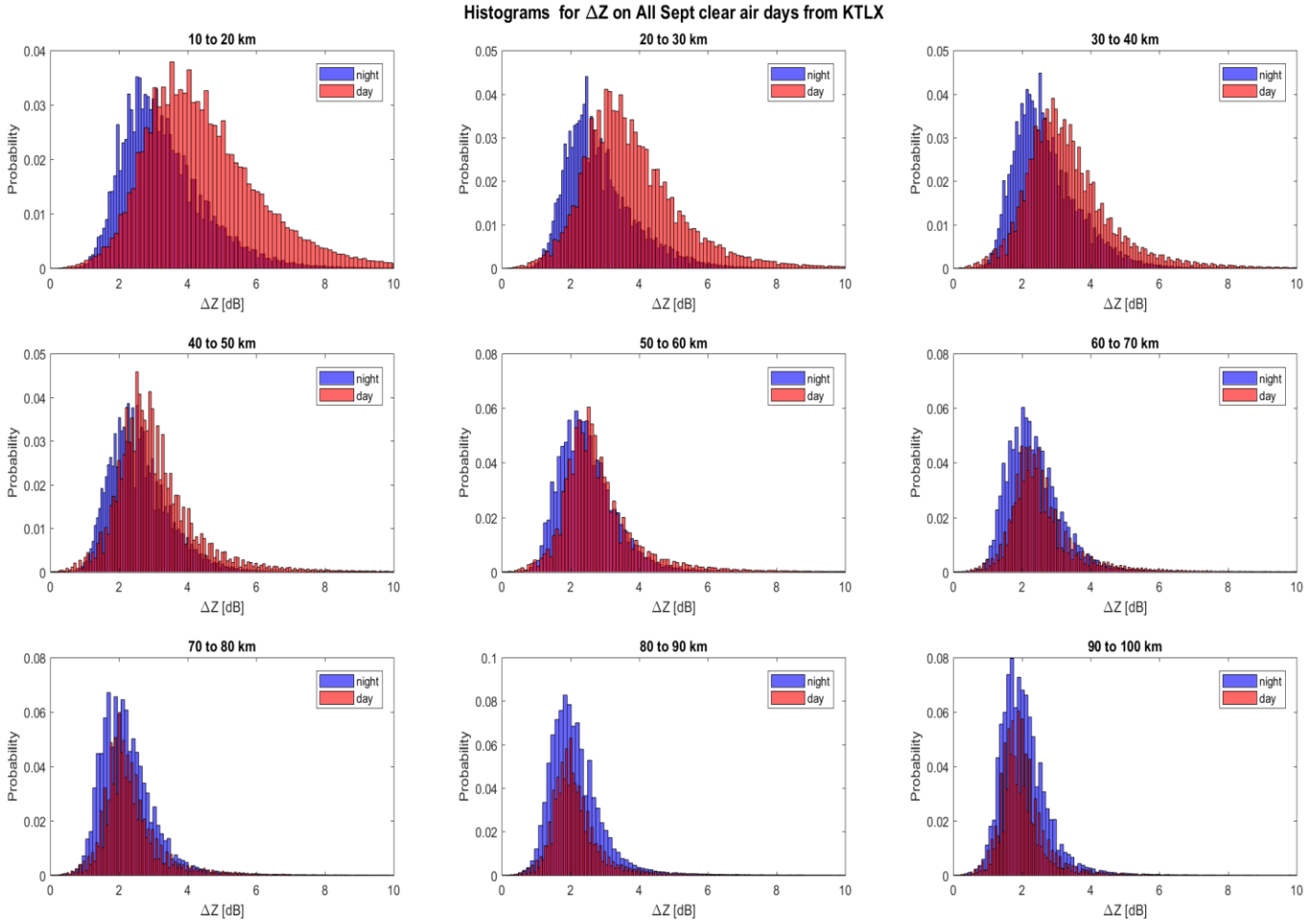

Fig. 3. 16 Histogram of ΔZ for Clear Air Days in September 2017

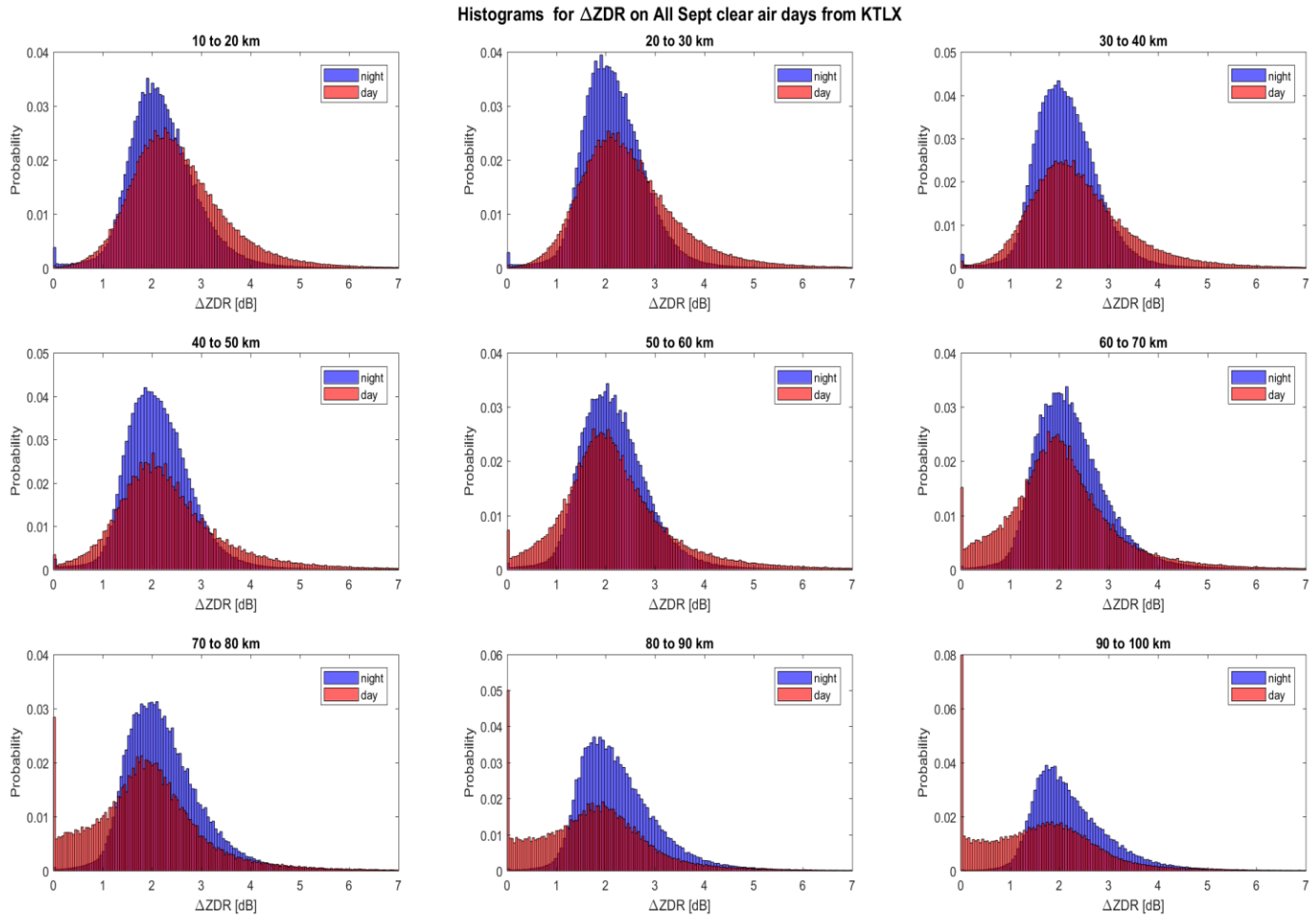

Fig. 3. 17 Z_{DR} texture ΔZ_{DR}

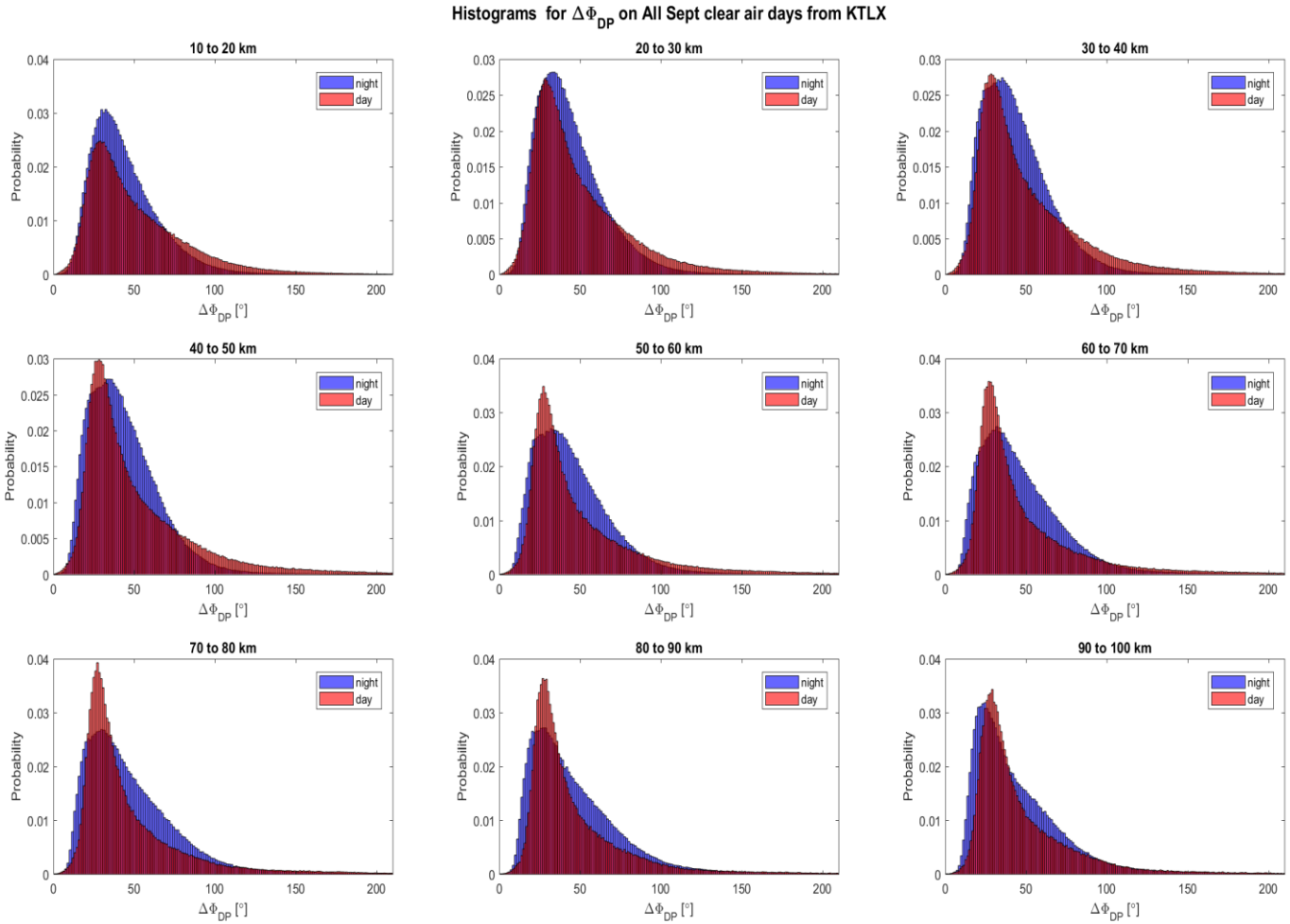

Fig. 3. 18 φ_{DP} texture $\Delta\varphi_{DP}$

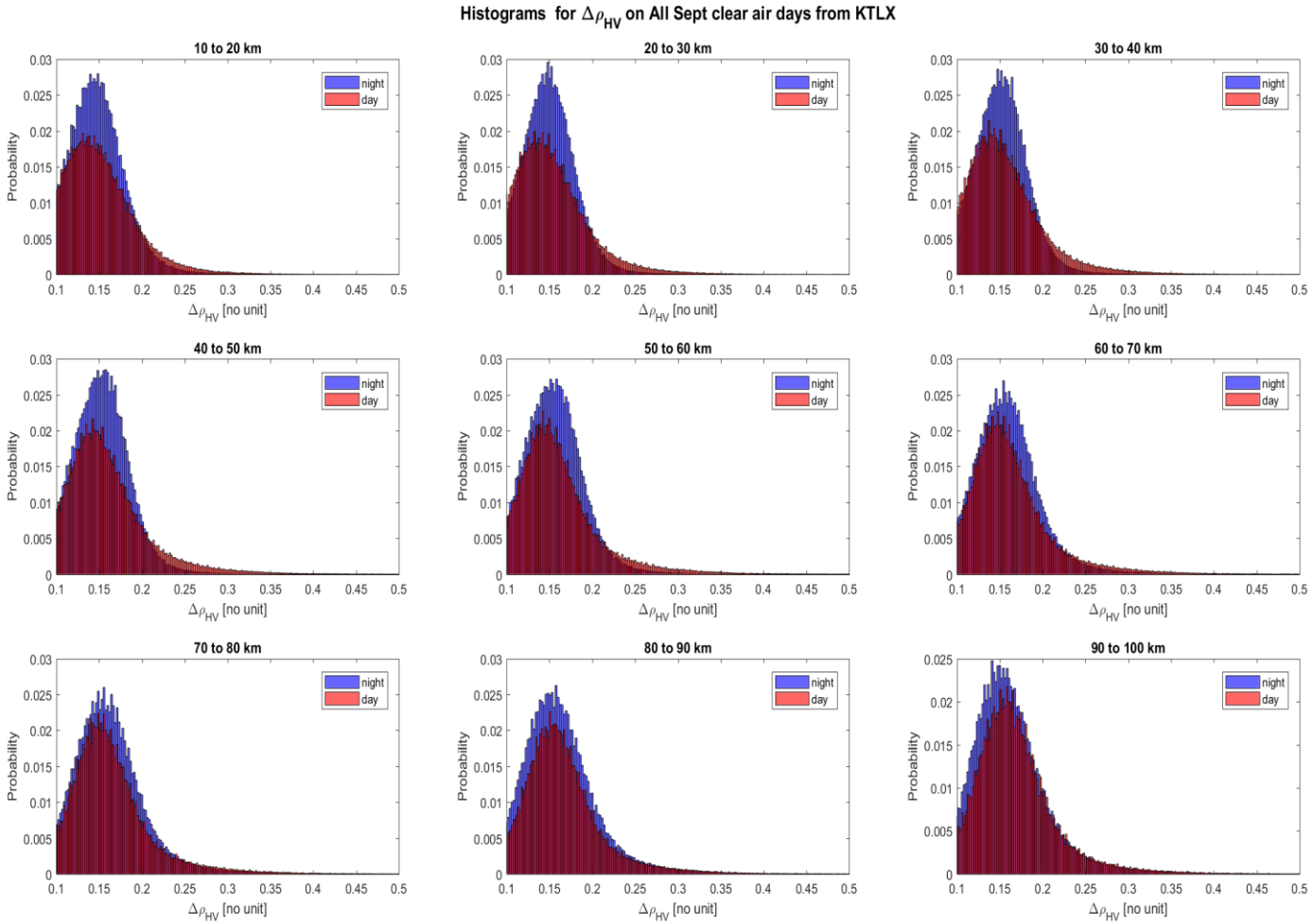

Fig. 3. 19 ρ_{HV} texture $\Delta\rho_{HV}$

Chapter 4

Fuzzy Logic Algorithm to distinguish bird and insect radar echoes

4.1 Introduction

Most radar classification algorithms work on the principle of fuzzy logic. Decisions are made by comparing measured properties of scatterers with previously acquired knowledge. Final class assignment is based on the level of consistency between the two. Fuzzy logic classification principles for weather radar targets were first explored by Straka & Zrnic (1993) and Straka J. M. (1996). Over time more refined routines have been developed by Zrnic & Ryzhkov (1999), Vivekanandan, et al. (1999), Liu & Chandrasekar (2000), Zrnic et al. (2001), Schuur et al (2003), Keenan (2003), Lim et al. (2005), Marzano et al. (2008), Gourlery et al. (2006) and Krause (2016). Radar measurements are affected by noise. Furthermore, all radar variables from birds experience resonance effects. A major advantage of fuzzy logic is that it considers many observations so the effects of noisy or resonant measurements are minimized.

The Hydrometeor Classification Algorithm (HCA) by Park et al (2008), currently used on NEXRAD also uses fuzzy logic principles to identify various classes of echoes. One of these classes is the "Biological Class", however the algorithm cannot classify its taxa. In this study, a bird/ insect fuzzy logic classification scheme based on observation of clear air echoes is presented. Results in the previous chapter were obtained for the dominant presence of birds during the night and insects in the day. The membership functions are derived directly from our observations. These functions are unique for every 10 km range interval considered. To the best of my knowledge, this is the first

time a fuzzy logic algorithm has been developed for separating bird and insect echoes. The algorithm was tested on two known cases of insects. Further testing for a complete day supports that daily reflectivity cycles (Martin, 2003) are caused by insects dominating day echoes and birds dominating night echoes.

The content of this chapter is as follows. First, a discussion on the general structure of the algorithm is presented in section 4.2 followed by the derivation of the membership functions and weights in section 4.3. Finally, test results are presented in greater detail in section 4.4.

4.2 General structure of the algorithm

Fig 4.1 below shows the general structure of the algorithm. It uses the 7 parameters previously found to have the best separation between birds and insects. They are Z, σ_v, Z_{DR}, φ_{Dp}, ρ_{HV}, ΔV and $\Delta\sigma_v$. The Doppler velocity V is not used because it depends on the azimuthal angle of the target relative to the radar, as such low V may just mean that the target velocity is almost perpendicular to the radar beam. Texture ΔV measures the variation of V over a contiguous area comprised of three successive radials. Since it compares neighboring radials, it is not as sensitive as V to the targets location. Also, birds flocks are usually contained in a region (usually one resolution volume) surrounded by other volumes which may not contain birds (may contain insects). As such, ΔV will be higher for areas with birds than areas without birds as discussed in the previous chapter. For these reasons, ΔV is used in the algorithm. Similarly, birds typically have large σ_v so regions with bird migration will possess higher $\Delta\sigma_v$ than regions with insects. Texture $\Delta\sigma_v$ is also used in the algorithm

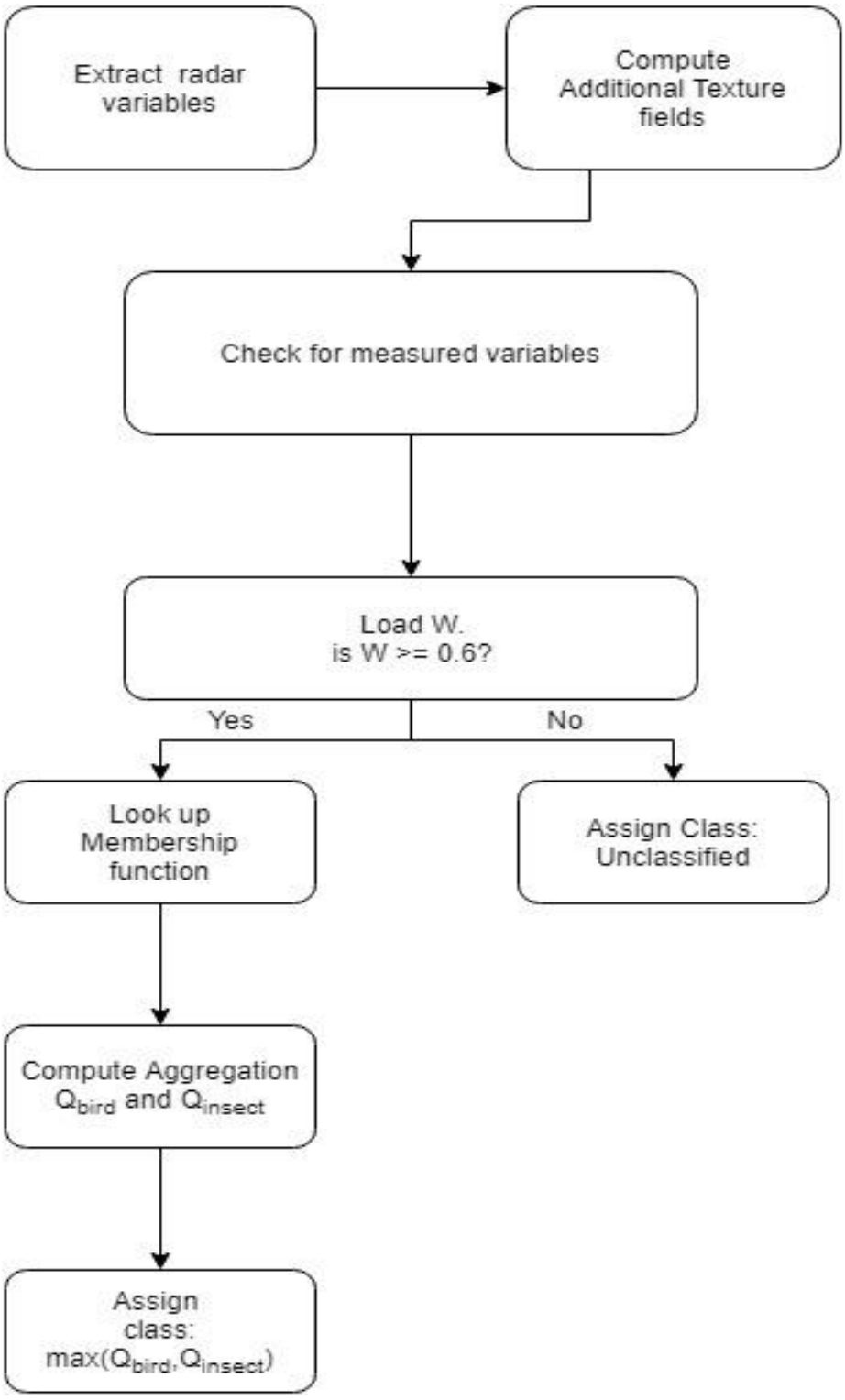

Fig. 4. 1 Flow chart of fuzzy logic algorithm

.

Two (2) classes of clear air echoes are defined for birds and insects. All gates outside the range considered for this project and gates without enough measurements are not classified. The likelihood of a range gate belonging to a class is measured as the Aggregation value. An additive aggregation Q_i is computed as (Park et al, 2008; Gourlery et al, 2006)

$$Q_i = \frac{\sum_{j=1}^{7} W_{ij} P^{(i)}(v_j)}{\sum_{j=1}^{7} W_{ij}} \quad , \tag{4.1}$$

where Q_i is the aggregation value of the *i*th class,

$P^{(i)}(v_j)$ is the membership of the *j*th variable to the *i*th class, and

W_{ij} are the weights of the *j*th variable and *i*th class

Additive aggregation is chosen for this algorithm because it is more resistant to noise or abnormal measurements. Other studies (Liu & Chandrasekar, 2000), (Lim, Chandrasekar, & Bringi, 2005) use a multiplicative aggregation procedure, however it can be easily biased by values near zero or that are extremely high. Another procedure is the "hybrid" aggregation, used by Zrnic et al 2001 and Schuur et al 2003. However, they have been found to be sensitive to Z biases caused by calibration uncertainties or attenuation (Gourlery et al., 2006).

After the aggregation for each class is computed, the final class is selected as the one with the maximum value. Gates are not classified if they are outside the considered range (10-100 km), or when the sum of weights of available (non NaN) variables fails to exceed a threshold of 0.6. This threshold ensures that classification of a range gate

proceeds only when the variables available can account for 60% of the total possible weight (1).

The last step in the algorithm is despeckling. It is unlikely that a radar volume filled with insects will be completely surrounded by birds. Despeckling considers a 3 by 3 window (or texture volume) over the classification output and changes the reference gate to be classified as a bird echo, only if all surrounding gates from the same elevation are classified are also classified as bird echoes. So, it is assumed that the reference gate had its non-bird characteristics due to fluctuation of radar returns.

4.3 Membership functions and Weights

The quality of a successful fuzzy logic algorithm depends on how well the membership functions describe the scatterers. Many studies use empirical knowledge or previous observations to form these functions. Zrnic et al (2001) used trapezoidal shapes to describe observed range of scatterer's values while Liu and Chandrasekar (2000) use continuously differentiable beta functions. In this study, membership functions are derived directly from the observed distributions for birds and insects. They are computed by first using the Gaussian kernel density estimation (Silverman, 1986), (Gourley et al., 2006) to estimate the probability density of data as shown below

$$\hat{f}(y) = \frac{1}{n\sigma\sqrt{2\pi}}\sum_{k=1}^{n} exp\left(-\frac{(y-x_k)^2}{2\sigma^2}\right) , \quad (4.2)$$

where $\hat{f}(y)$ is the probability density function

x_k is the kth observation of variable x

n is the total number of data points

σ is the bandwidth chosen using Silverman's rule, i.e

$$\sigma = 1.06\, SD\, n^{-\frac{1}{5}} \quad , \tag{4.3}$$

where SD is the standard deviation of the observed variable, x. This density estimation is repeated for every *i*th class of *j*th variable for every range interval. The resulting function is essentially a smoothed histogram of the radar data. Finally, membership functions $P^{(i)}(v_j)$ are derived by normalizing $\hat{f}(y)$ so that the maximum is one. The advantage of this method is the resulting functions have the same distribution as the data and highlight unique features of the data (like Z_{DR} aggregating at 8 dB). Fig 4.2 – 4.8 show the membership functions for ΔV, $\Delta\sigma_v$, φ_{Dp} ,ρ_{HV}, σ_v, Z_{DR} and Z respectively. Functions for bird echoes are in blue while those for insect echoes are in red.

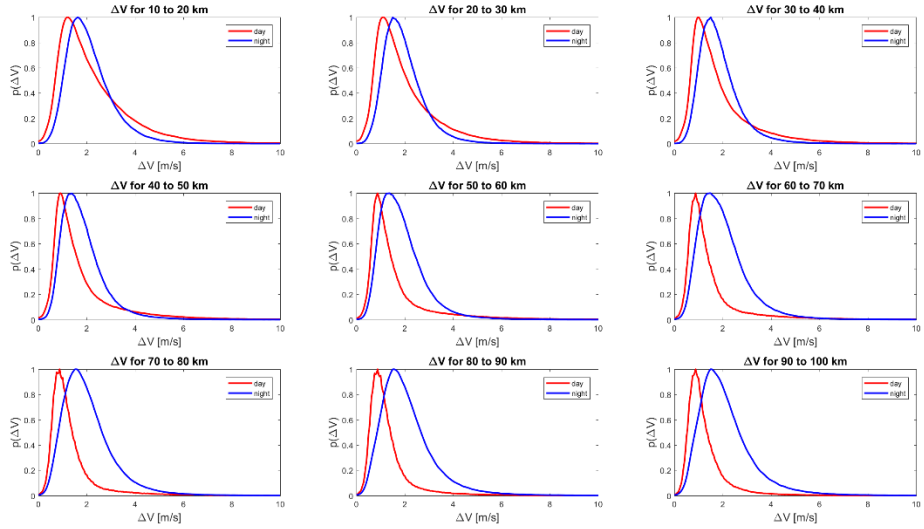

Fig. 4. 2 Membership functions for ΔV

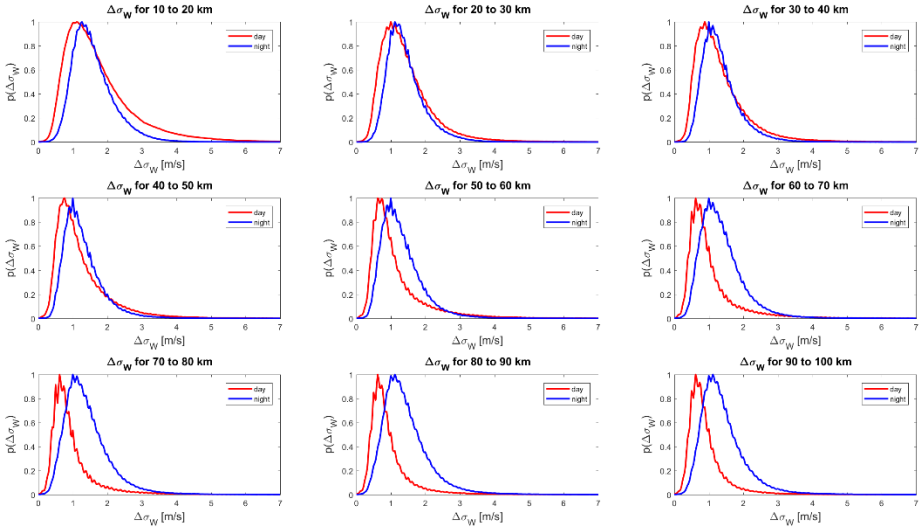

Fig. 4. 3 Membership functions for $\Delta\sigma_v$

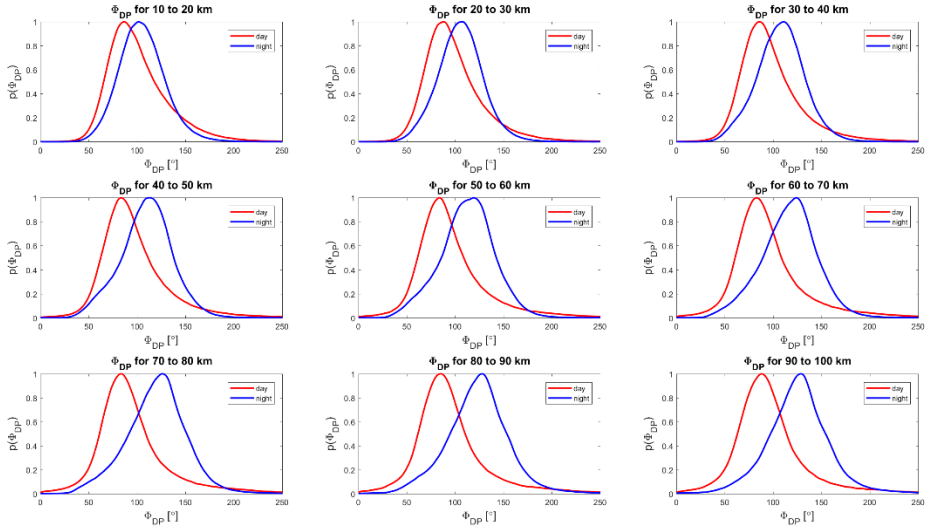

Fig. 4. 4 Membership functions for φ_{Dp}

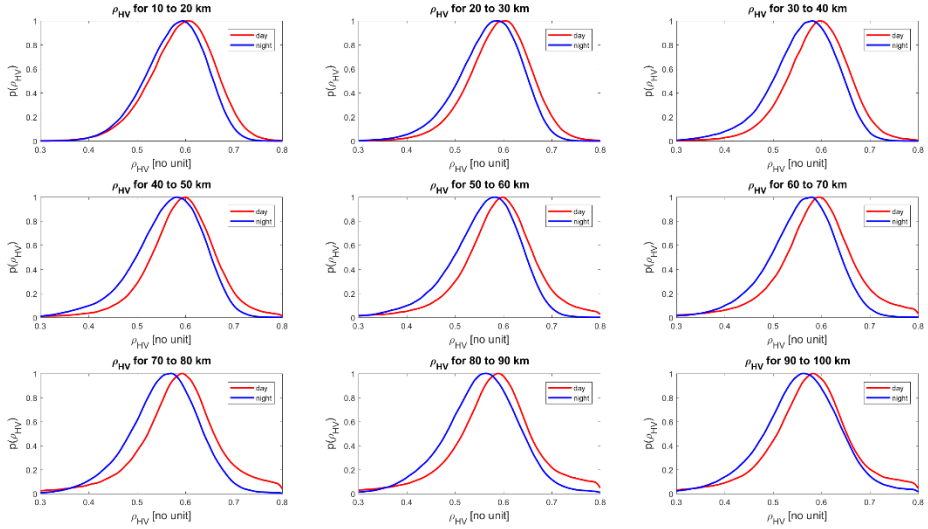

Fig. 4. 5 Membership functions for ρ_{HV}

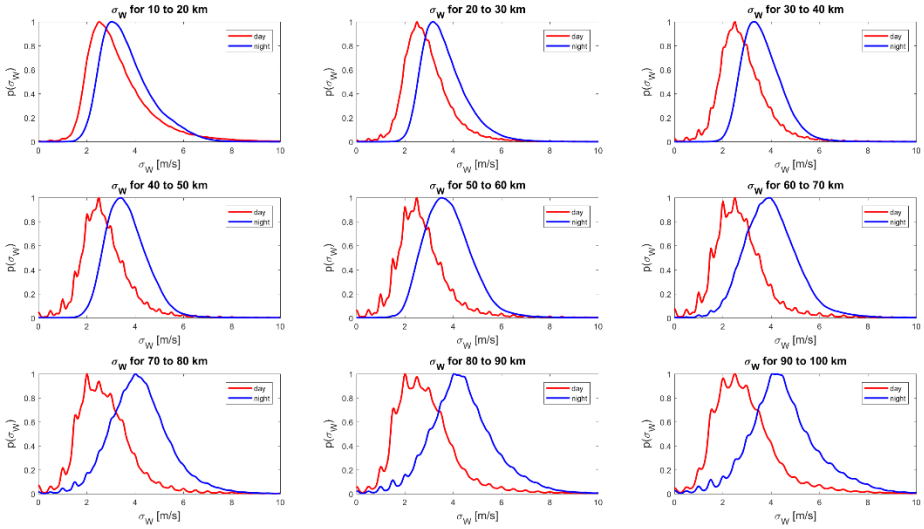

Fig. 4. 6 Membership functions for σ_v

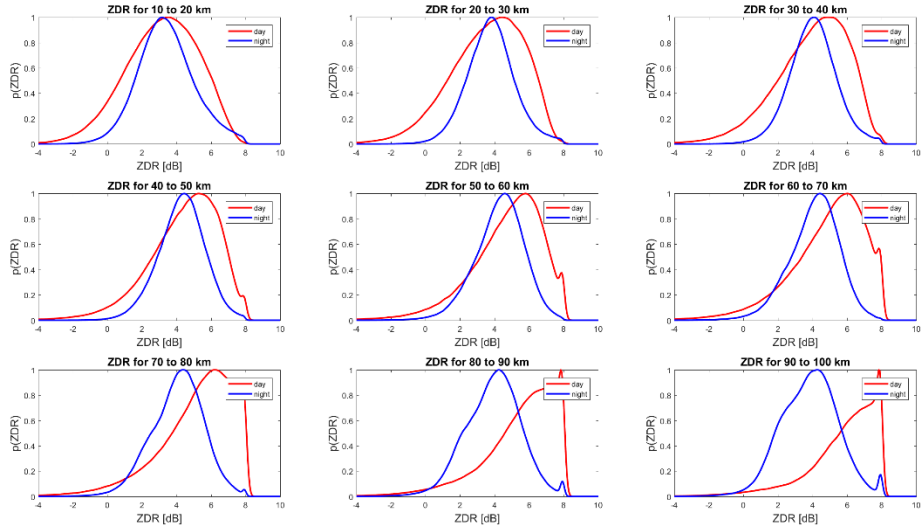

Fig. 4. 7 Membership functions for Z_{DR}

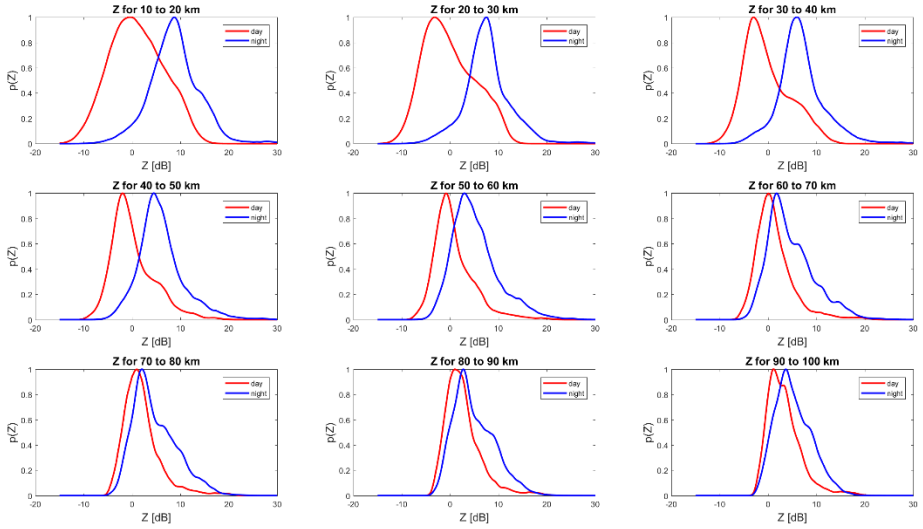

Fig. 4. 8 Membership functions for Z

The Weights defined in (4.1) determine the extent each variable play in the classification procedure. They were computed based on the degree of overlap between probability densities of the two classes (Park et al., 2007) as shown below.

$$W_l = \frac{1}{A_l}\sum_{j=1}^{N}\frac{1}{A_j} \quad , \tag{4.4}$$

where N is the number of variables considered and A is the overlapping area between bird and insect distribution. It can be seen from 4.4 that the weight is inversely proportional to overlapping area Thus, if a variable has strong overlap between bird and insect density, it is assigned a low weight and vice versa. For example, fig. 4.9 shows the distribution for φ_{DP} at the 40 -50 km range. The overlapping region, A_l (highlighted in pink) was found to be 0.68. This procedure was repeated for all j variables at the same range. The final weight of 0.12 is found by substituting these areas in equation

(4.4) and then normalizing so that the weights sum up to one. Table 4.1 below shows the weights for all variables and ranges considered.

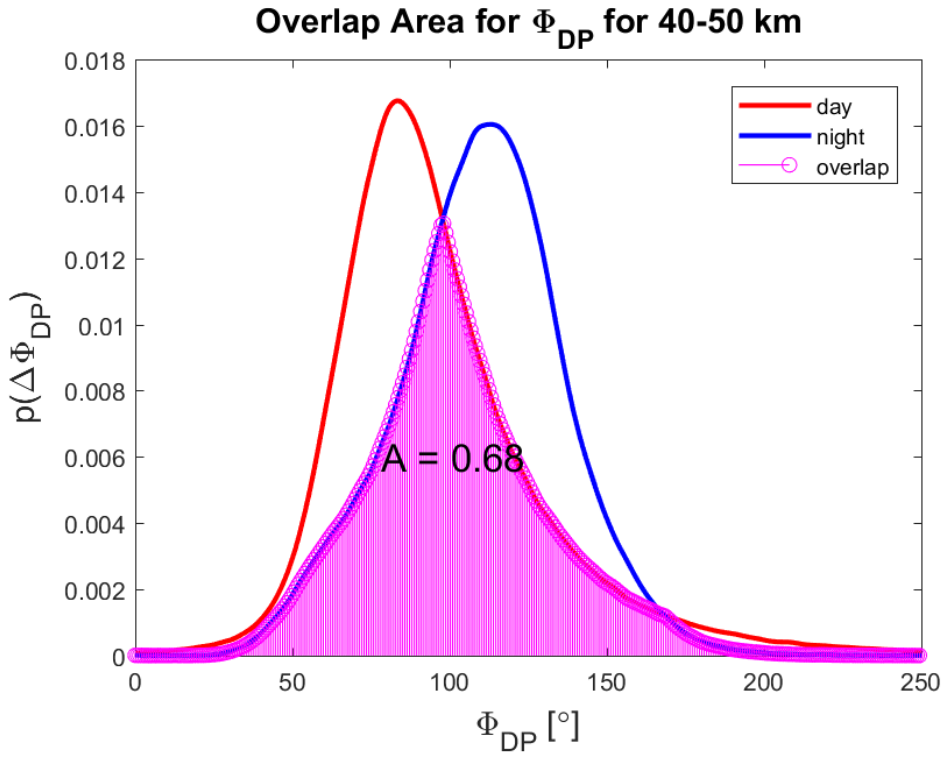

Fig. 4. 9 Area of Overlapping region for φ_{DP} for 40 – 50 km

Table 4. 1 Weights of all variables and ranges

		Range Interval								
Parameter		**1**	**2**	**3**	**4**	**5**	**6**	**7**	**8**	**9**
	ΔV	0.13	0.13	0.13	0.13	0.13	0.13	0.13	0.13	0.13
	$\Delta\sigma_v$	0.13	0.12	0.11	0.12	0.13	0.14	0.15	0.15	0.15
	φ_{DP}	0.13	0.13	0.13	0.14	0.15	0.15	0.16	0.16	0.15
	ρ_{HV}	0.12	0.11	0.11	0.11	0.11	0.11	0.11	0.10	0.09
	σ_v	0.14	0.15	0.16	0.17	0.18	0.18	0.18	0.18	0.17
	Z_{DR}	0.13	0.13	0.12	0.12	0.13	0.13	0.14	0.15	0.17
	Z	0.23	0.24	0.23	0.21	0.17	0.13	0.12	0.11	0.11

where range interval 1 is 10-20 km, 2 is 20-30 km, 3 is 30-40 km, 4 is 40-50 km, 5 is 50 - 60 km, 6 is 60 - 70 km, 7 is 70-80 km, 8 is 80-90 km, and 9 is 90-100 km.

4.4 Classification Results

4.4.1 Insect Case

Data for the insect test case was obtained from the US Department of Agriculture (USDA) in Texas which monitors the activity of insects in many states including Oklahoma. A large population of Monarch butterfly, *Danaus plexippus* was confirmed on 19th July, 2013, 17 -19 UTC (12 – 14 CDT) and 1st November, 2013, 22 -23 UTC (17-18 UTC).

For the July 2013 case, the algorithm was applied to a PPI from KLTX collected at 12:46:04 CDT. The classification result is shown in fig 4.10 below. The algorithm detected 87.9 % of echoes to be insects and 12.1 % to be birds. This correlates with the USDA's observation of a large population of Monarch butterflies. It can also be observed that birds are mostly isolated echoes consistent with the tendency for birds to aggregate within few resolution volumes. Results for 17:30:06 CDT on 1st November, 2013 is shown in fig. 4.11. Insects were also found to dominate echoes at 76.5%. Bird echoes are also seen as isolated targets.

4.4.2 Daily Cycle Case

Observations of clear air Reflectivity show a daily cycle (Martin, 2003) with dips at sunrise and sunset and clear change in scattering mechanism between day and night. In this section data from a 24-hour cycle, between 19 CDT on 16th September, 2015 and 18 CDT, 17th September, 2015 is classified to explore this cycle. The results are presented in fig 4.12 – 4.15.

Insects initially dominate echoes with 81.9% at 19 CDT for the first day (fig 4.12) but soon after its area decreases till it dips at 3 CDT, the next day with 51.11 %. (fig 4.13).

After this point, insect percentage rises continuously till it reaches its maximum at 9 CDT (early morning) with 93.2%. Generally, day time (9 CDT to 18 CDT), insect percentage is high with a mean of 85.7% seen in fig 4.14 & 4.15. Night time (21 CDT to 6 CDT) on the other hand, has lower mean insect percentage of 59% seen in fig 4.12 & 4.13. Day break (6 CDT) is observed to be the inflection point with 71% of echoes identified as insects

Bird abundance rises from 18% at 21 CDT on 16th September 2017 (fig 4.12). This trend continues up till 4 CDT (fig 4.12) the next day with 46.8%. Peak values are recorded at night (between 21 CDT and 4 CDT) with an average of 43.3% seen in fig 4.12 & 4.13. After this point, bird percentage falls for the rest of day time. 9 – 18 CDT have generally low values with an average of 14.3%. These results show that insects dominate day echoes while birds dominate nocturnal echoes. Results also show a distinct change in behavior of birds and insects at sunrise (6 CDT) and sunset (18 CDT).

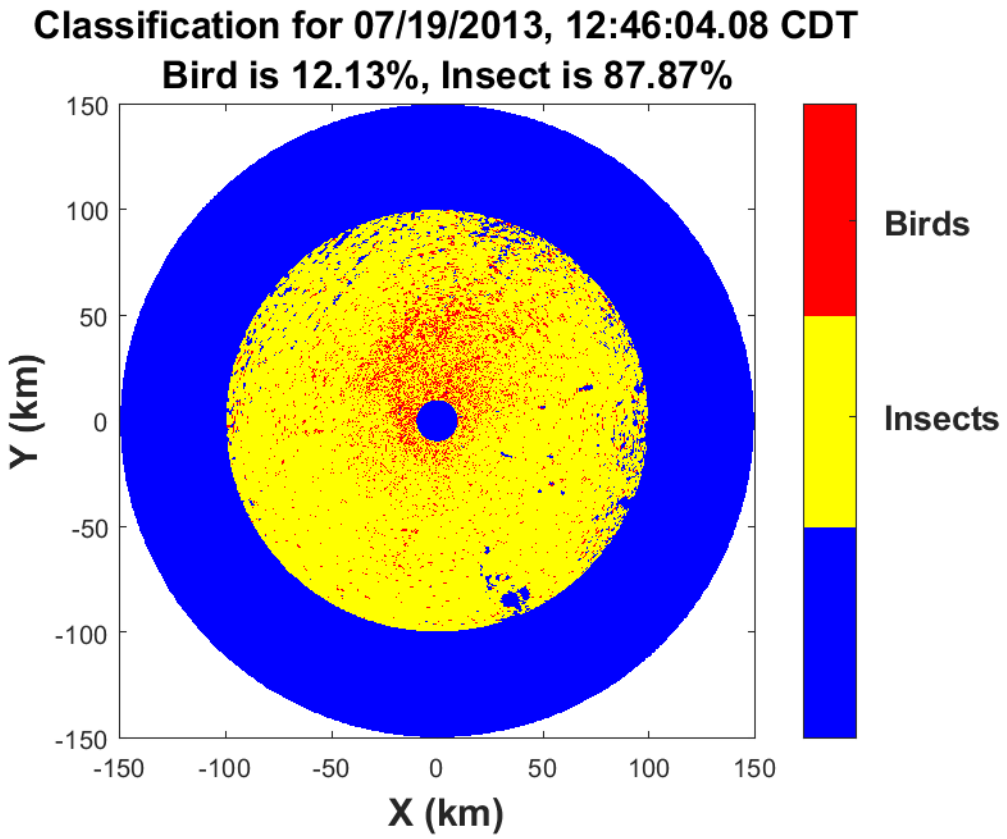

Fig. 4. 10 Classification result for 19th July, 2013 at 12:46:04 CDT.

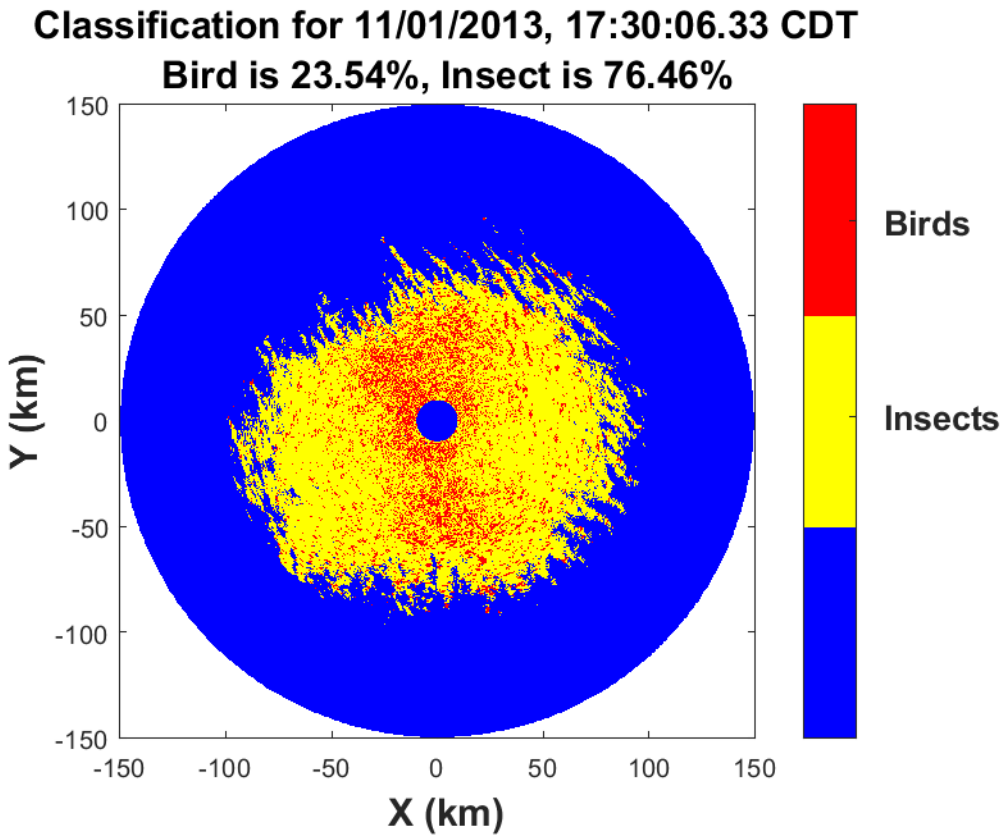

Fig. 4. 11 Classification result for 1st November, 2013 at 17:30:06 CDT

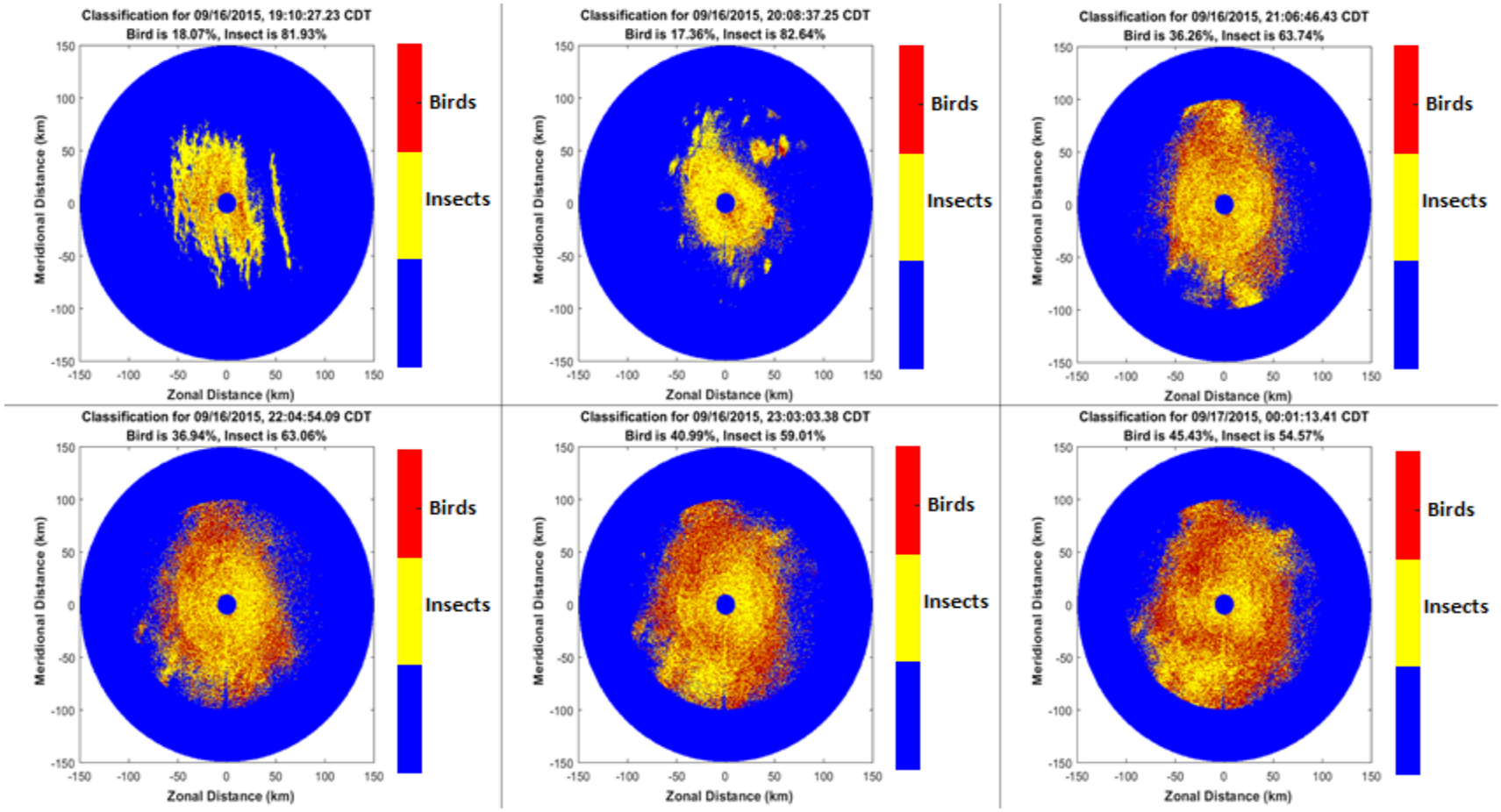

Fig. 4. 12 Classification result for 19 CDT, 16 September, 2015 to 1 CDT, 17 September, 2015

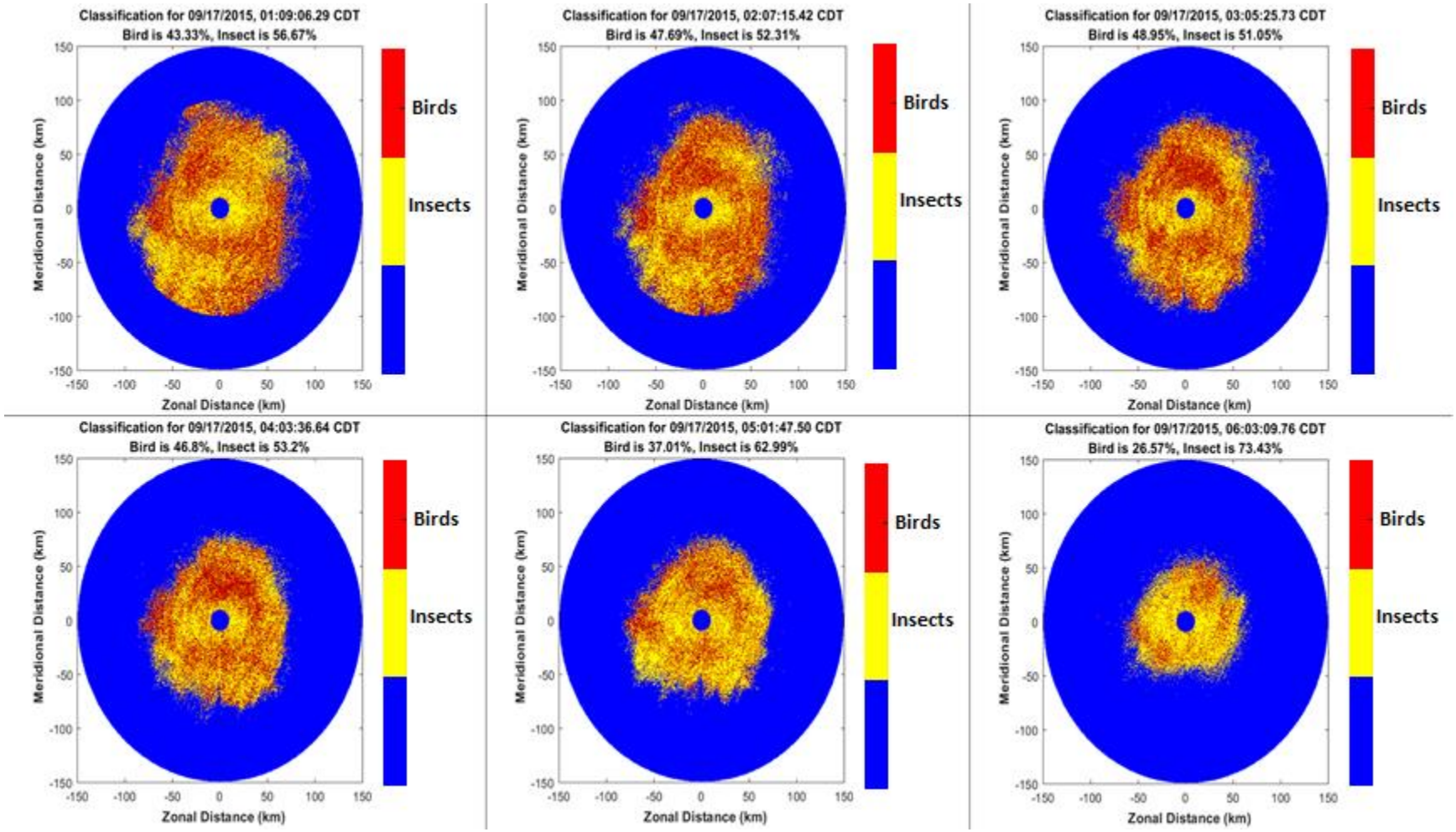

Fig. 4. 13 Classification result for 17 Sept, 2015, 1 CDT to 6 CDT

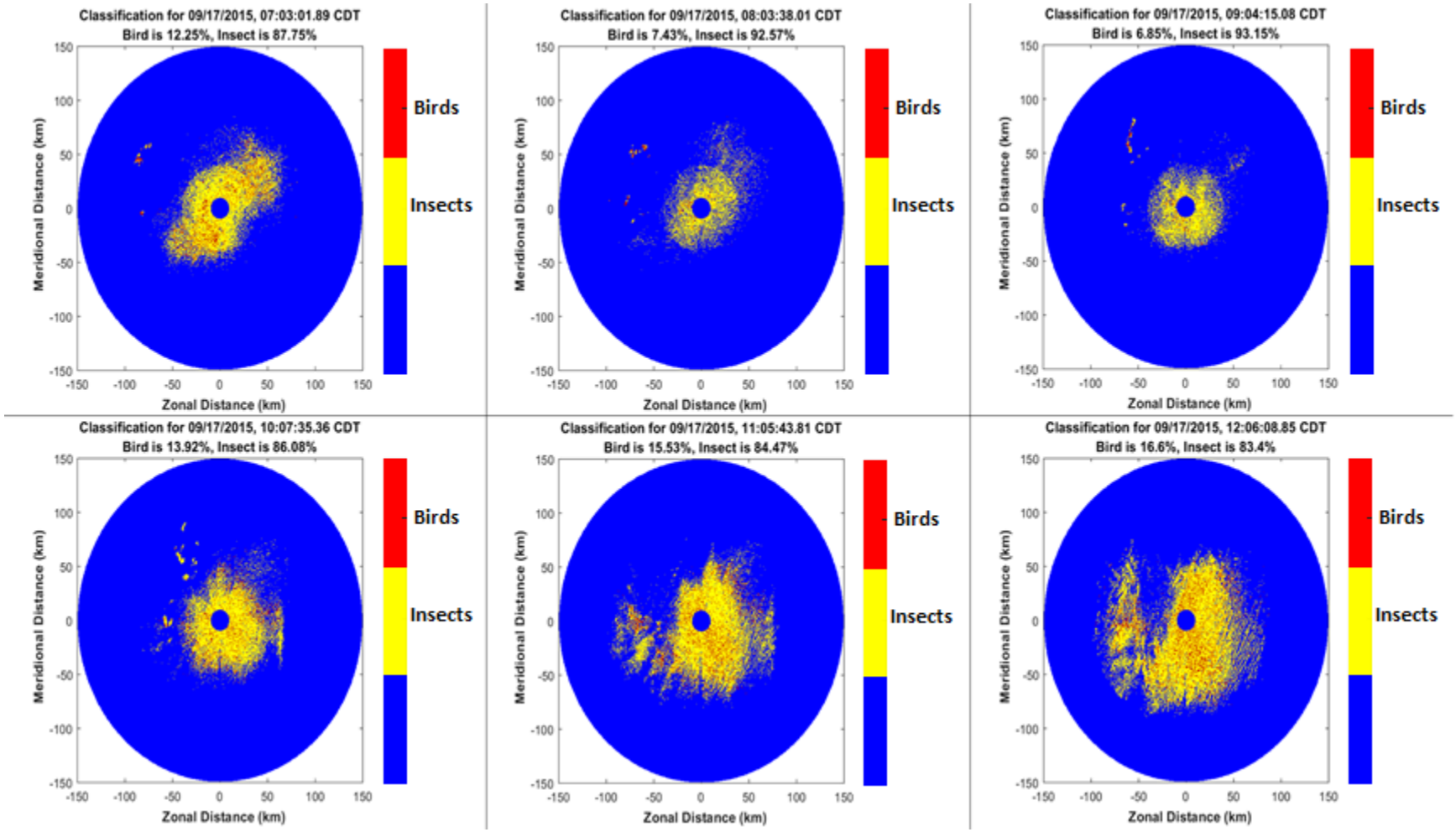

Fig. 4. 14 Same as 4.13 but for 7 CDT to 12 CDT

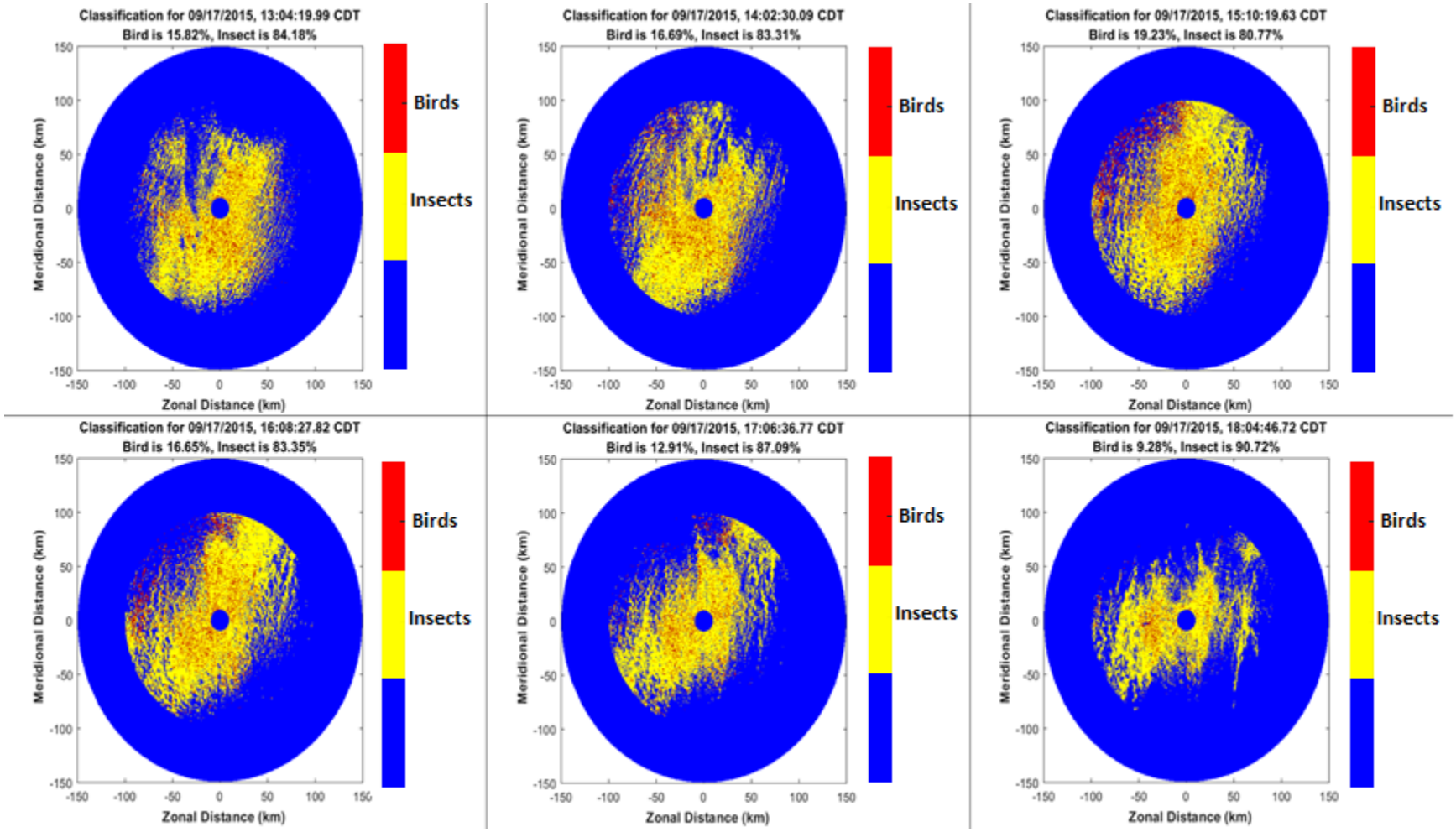

Fig. 4. 15 Same as 4.14 but for 13 CDT to 18 CDT

Chapter 5
Summary and Conclusions

The current WSR-88D's Hydrometeor Classification Algorithm (HCA) does not distinguish radar echoes from birds and insects. The HCA currently has one class "Biological" for flying birds, bats, and insects. The recognition of bird and insect radar echoes is important for meteorology, aviation, ecology, biology, and agriculture. The WSR-88D radars estimate the wind velocities using observations in "clear air", i.e., in situations free from precipitation. This is accomplished using the Velocity-Azimuth-Display (VAD) technique. Birds are active flyers and their velocities deviate from the wind significantly. Therefore, the Doppler velocities of birds cannot be used for the estimation of the wind. On the other hand, insects are almost passive flyers and they may be used as wind tracers. Selecting radar resolution volumes with insects can be useful for meteorology for the wind estimation via the VAD.

Flying birds are a major hazard for aviation while insects are benign. Therefore the radar detection of birds can be useful in preventing collisions of birds with aircrafts and helicopters. Furthermore, distinguishing bird and insect radar echoes could be useful for agriculture for the pest management. The parameters of bird migration such as the flight direction, height, and velocity as well as number concentration of species are also of interest for biology and ecology.

The dual polarization WSR-88Ds deliver 6 radar variables for each radar resolution volume: reflectivity (Z), Doppler velocity (V), spectrum width (σ_v), differential reflectivity (Z_{DR}), differential phase (φ_{DP}), and correlation coefficient

(ρ_{HV}). Our radar observations in "clear air" show that the values of radar variables change with range from radar. This is probably because various species fly at various heights. Therefore, the range dependence should be included into an algorithm for distinguishing bird and insect echoes. We have limited our analysis by ranges up to 100 km where the range dependence of radar variables is sufficiently strong. The developed algorithm could be applied for an airport terminal area, which is 50-60 km from an airport, if the WSR-88D is sufficiently close to the airport.

It is known from ornithology and entomology that in the migration periods, birds fly primarily at night and insects may fly throughout the day, but preferable flight time is during the day. Data collected from clear air days have been analyzed at daytime and nighttime. The distributions of the values of all 6 radar variables and their spatial textures have been obtained for 22 days in September 2017 for day and night times. Birds are larger, faster, fly more independently, more dense and have greater variation in the mentioned features compared to insects. These properties are observed with the distribution of nocturnal echoes having a higher median Z, V, σ_v, φ_{DP} and lower median ρ_{HV} than the day echoes. The spatial texture ΔV and $\Delta\sigma_v$ which measure the spatial variability of scatterer velocities are also higher for night time providing more evidence in favor of bird abundance in nocturnal echoes.

The distributions of all 6 radar variables and corresponding 6 spatial textures ΔZ, ΔV, $\Delta\sigma_v$, $\Delta\varphi_{DP}$, ΔZ_{DR}, and $\Delta\rho_{HV}$ have been obtained for the nights and days. After data analysis, a fuzzy logic classification algorithm is developed to delineate birds and insects in clear air echoes. The membership functions are derived using the Gaussian kernel approximation on observed data as in Gourley *et al.* 2016. Weights are

objectively defined using the degree of separation between classes (as in Park et al., 2007), so that parameters that show the clearest separation between night and day have the most effect on classification. Five radar products (Z, Z_{DR}, σ_v, φ_{DP} and ρ_{HV}) as well as two derived products ΔV and $\Delta\sigma_v$ were chosen for use in the algorithm based on observed separation between distributions of classes.

The algorithm was tested on two confirmed cases with a high population of Monarch butterfly, *Danaus plexippus* on 19th July, 2013, 12:46:04 CDT and 1st November, 2013 on 17:30:06 CDT. Data was obtained from the US Department of Agriculture (USDA) in Texas which monitors insect activity in many states including Oklahoma. For the July case, 87.9% of echoes were .classified as insects while 12.1% were classified as birds. For the November case, 76.5% of echoes were classified as insects and 23.5% were classified as birds. Insect echoes were also distributed over large volumes while birds occurred mainly as isolated volumes. These results led to the following conclusions

- Strong correlation between classification results and observations by the USDA proves that the distribution used to characterize insect membership functions are indeed insects. Thus, insects were the cause of day time clear air echoes for September, 2017
- It is reasonable to expect birds to be in some resolution volumes for the 90 km (10 to 100 km from the radar) radius considered. As such, the percentage of insects found should be very close to the actual amount. It is impossible to determine an exact probability of detection since the taxa could not be confirmed from other independent sources.

The algorithm was also tested for a 24-hour period between 19 CDT on 16th September, 2015 and 18 CDT, 17th September, 2015. Insects were found to dominate echoes between 9 CDT and sunset on 17th September, 2015 with an average of 85.7% of classified echoes. After sunset on 16th September, insect percentage falls rapidly with lowest values between 21 CDT and 6 CDT, with an average of 59%. Bird abundance peaked between 21 CDT on 16th September, 2015 and 4 CDT the next day with an average of 43.3%. After sunrise, bird abundance falls rapidly throughout the rest of day time (9 -18 CDT) with an average of 14.3%. A major feature of these results is that day break (6 CDT) marks the inflection point between high and low values for birds and insects. These findings explain the daily cycle of reflectivity observed by (Martin, 2003). Insects are clearly most abundant during the day and birds during the night at migration periods. Sunrise and Sunset are also found to be inflection points in the dominance of birds or insects in the atmosphere.

The following new features have been utilized in the algorithm:

- Range dependence for the radar variables and their textures has been considered,
- All 6 available radar variables and their spatial textures have been analyzed,
- Five radar variables and two texture parameters have been found to contribute the most to the separation of radar echoes from birds and insects,
- Probabilities (distributions) of certain radar variables have been obtained for 6 parameters and their 6 textures,
- Fuzzy logic algorithm to distinguish bird and insect echoes has been developed,

- Two cases with confirmed domination of insects have been tested by the algorithm. The strong presence of insects on those days was confirmed by US Department of Agriculture.

A few areas can be improved upon in future studies. The wind contributes a lot to measured radial velocity and birds/insects have distinct behavior in relation to the wind. A new algorithm parameter can be derived for the deviation of radial velocity from wind velocity. It is expected that birds will have higher values than insects. Furthermore, the radar variables as functions of azimuth can be reoriented relative to the wind before data processing to properly characterize their dependence on the wind. Independent sources of information about birds and insects in the radar resolution volume are also needed. A camera on an unmanned aerial vehicle could be very helpful for the verification of scatterers in the radar resolution volume. Further tests can be performed by tracking insect patterns over a time to estimate the wind direction and compare with other measurements of wind direction.

References

Bachmann, S., & Zrnic, D. (2006). Spectral Density of Polarimetric Variables Separating Biological Scatterers in the VAD Display. *Journal of Atmos. and Ocean. Tech.*

Battan, L. (1973). *Radar Observations of the Atmosphere.* University of Chicago Press.

Browning, K., & Atlas, D. (1966). Velocity characteristics of some clear-air dot angels. *J. Atmos. Sci*, 592-604.

Crawford, A. B. (1949). Radar reflections in the lower atmosphere. *Proceedings of the I.R.E.*, (pp. 404-5).

Doviak, R., & Zrnic, D. (1993). *Doppler Radar and Weather Observations. Second Edition.* New York: Dover Publications.

Drake, V. A. (1984). The vertical distribution of macro-insects migrating in the nocturnal boundary layer: a radar study. *Bound. Lay. Meteor.*, 353-74.

Drake, V. A. (1985). Radar observations of moths migrating in a nocturnal low-level jet. *Ecol. Entomol.*, 259-65.

Dual-Polarization Radar Principles and Systems Operations. (2018). Retrieved from Warning Decision Training Branch Web site: https://training.weather.gov/wdtd/courses/dualpol/documents/DualPolRadarPrinciples.pdf

Eastwood, E. (1967). *Radar Ornithology.* Methuen & Co., Ltd.

Federal Aviation Administration. (2016). *Wildlife strikes to Civil Aircraft in the United States 1990 -2015, Report of the Associate Administration or Airports.* National Wildlife Strike Database Serial Report Number 22.

Friend, A. (1939). Continous cetermination of air-mass boundaries by radio. *Bull. Amer. Met. Soc*, 202-5.

Gauthreaux, S., & Belser, C. (1998). Display of bird movements on the WSR-88D: patterns and quantification. *Wea. and Fore.*, 453-64.

Gauthreaux, S., Mizrahi, D., & Belser, C. (1998b). Bird migration and bias of WSR-88D wind estimates. *Wea. and Fore.*, 465-81.

Geerts, B., & Miao, Q. (2005). Airborne Radar Observations of the Flight Behaviour of Small Insects in the Atmospheric Convective Boundary Layer. *Environmental Entomology*, 361-77.

Gossard, E., & Strauch, R. (1983). Radar Observations of Clear Air and Clouds. *Elsevier*.

Gourlery, J. J., Tabary, P., & Parent du Chatelet, J. (2006). A Fuzzy Logic Algorithm for the Separation of Precipitating from Nonprecipitating Echoes Using Polarimetric Radar Observations. *Amer. Meteor. Soc.*

Hardy, K., & Glover, K. (1966). 24 hour history of radar angel activity at three wavelengths. *Twelfth Conference on Radar Meteorology.* Norman, Oklahoma.

Hardy, K., & Katz, I. (1969). Probing the atmosphere with high power, high resolution radars. *Proceedings of the IEEE*, (pp. 468-80).

Jungbluth, K., Belles, J., & Schumacher, M. (1995). Velocity contamination of WSR-88D and wind profiling data due to migrating birds. *Preprints 27th Conference on Radar Meteorology*.

Keenan, T. D. (2003). Hydrometeor classification with a C-band polarimetric radar. *Aust. Meteor. Mag.*, 23-31.

Krause, J. M. (2016). A Simple Algorithm to Discriminate between Meteorological and Nonmeteorological Radar Echoes. *Amer. Meteor. Soc.*

Kropfli, R. A. (1986). Single Doppler radar measurements of turbulence profiles in the convective boundary layer. *J. Atmos. Ocean. Tech.*, 305-14.

Kropfli, R., Katz, I., Konrad, T., & Dobson, E. (1968). Simultaneous radar reflectivity measurements and refractive index spectra in the clear atmosphere. *Radio Sci.*, 991-4.

Kumjian, M. R. (2013). Principles and applications of dual-polarization weather radar. Part I: Description of the polarimetric radar variables. *J. Operational Meteor.*

Lane, J., & Meadows, R. (1963). Simultaneous radar and refractometer soudings of the troposphere. *Nature*, 35-6.

Lim, S., Chandrasekar, V., & Bringi, V. (2005). Hydrometeor classification system using dual-polarization radar measurements: Model improvement and in situ verification. *IEEE Trans. Geosci. Remote Sens.*, 792-801.

Liu, H., & Chandrasekar, V. (2000). Classification of Hydrometeors based on polarimetric radar measurements: Development of fuzzy logic and neuro-fuzzy systems and in situ verification. *J. Atmos. Oceanic Technol.*, 140-164.

Martin, W. (2003). *Measurements and Modelling of the Great Plains low-level jet.* Oklahoma: University of Oklahoma Graduate College.

Marzano, F., Scaranari, D., Montopoli, M., & Vulpiani, G. (2008). Supervised classification and estimation of hydrometeors from C-band dual-polarized radars: A Bayesian approach. *IEEE Trans. Geosci. Remote Sens.*, 85-98.

Mie, G. (1908). Beiträge Zur Optik Trüber Medien, Speziell Kolloidaler Metallösungen. *Annalen der Physik*, 377- 445.

Miller, P., Barth, M., Smart, J., & Benjamin, L. (1997). The extent of bird contamination in the hourly winds measured by the NOAA profiler network: results before and after implementation of the new bird contamination quality control check. *Preprints, 1st Symposium in Integrated Observing Systems* (pp. 138-44). Long Beach, CA: Amer. Meteor. Soc.

NOAA's National Weather Service Radar Operations Center. (n.d.). Retrieved from https://www.roc.noaa.gov/WSR88D/Maps.aspx

O'Bannon, T. (1995). Anomalous WSR-88D wind profiles - migrating birds? *Preprints, 21st Conference on Radar Meteorology*.

Palmer, R., Bodine, D., Kumjian, M., Cheong, B., Zhang, G., Cao, Q., . . . Wang, Y. (2011). Observation of the 10 May 2010 Tornado Outbreak using OU-PRIME: Potential for New Science with High Resolution Polarimetric Radar. *American Meteorological Society*.

Park, H., Ryzhkov, A. V., S., Z. D., & K., K. (2007). Optimization of the Matrix of Weights in the Polarimetric algorithm for classification of radar echoes. *33rd Conf. on Radar Meteorology*. Cairns, QLD, Australia: Amer. Meteor. Soc.

Park, H., Ryzhkov, A. V., Zrnic, D. S., & Kim, K. (2008). The Hydrometeor Classification Algorithm for the Polarimetric WSR-88D: Description and Application to an MCS. *Weather and Forecasting*.

Patterson, T. (2016, September 12). *CNN*. Retrieved from CNN website: https://www.cnn.com/2016/09/09/us/sully-sullenberger-miracle-hudson-bird-strike-prevention/index.html

Probert-Jones, J. (1962). *The Radar Equation in Meteorology.* Quart. J. Roy. Meteor. Soc.

Radar Operations Center. (n.d.). Retrieved from NOAA's National Weather Service Radar Operations Center: https://www.roc.noaa.gov/WSR88D/Engineering/NEXRADTechInfo.aspx)

Riley, J. (1975). Collective orientation in night-flying insects. *Nature*, 113-4.

Schaefer, G. W. (1976). Radar observations of insect flight. *Insect Flight*.

Schuur, T. J., Ryzhkov, A. V., & Heinselman, P. L. (2003). *Observations and classifications of echoes with the polarimetric WSR-88D radar.* Norman, OK: NOAA/National Severe Storms Laboratory Rep.

Seidenman, P., & Spanovich, D. (2016). *How Bird Strikes Impact Engines*.

Silverman, B. W. (1986). Density Estimation for Statistics and Data Analysis. *Monographs on Statistics and Applied Probability*.

Skolnik, M. (2001). *Introduction to Radar Systems.* McGraw-Hill.

Stepanian, P., Horton, K., Melnikov, V., Zrnic, D., & Gauthreaux Jr, S. (2016). Dual polarization radar products for biological applications. *Ecosphere*.

Straka, J. M. (1996). Hydrometeor fields in a supercell storm as deduced from dual-polarization radar. *Preprints, 18th Conf. on Severe Local Storms* (pp. 551-54). San Francisco, CA: Amer. Meteor. Soc.

Straka, J., & Zrnic, D. (1993). An algorithm to deduce hydrometeor types and contents from multiparameter radar data. *Preprints, 26th Conf. on Radar Meteorology* (pp. 513-516). Norman, OK: Amer. Meteor. Soc.

U.S. Department of Commerce; National Oceanic and Atmospheric Administration. (2016). *Federal Meteorology Handbook No. 11: WSR-88D Meteorological Observations. Part A System Concepts, Responsibilities and Procedures.* Washington, DC.

van de Kamp, D., Ralph, F., Barth, M., Miller, P., Smart, J., & Benjamin, L. (1997). The new bird contamination quality control check applied to hourly winds from NOAA's profiler network. *Preprints, 28th Conference on Radar Meteorology.* Austin, Texas: Amer. Meteor. Soc.

Vivekanandan, J., Zrnic, D. S., Ellis, S., Oye, D., Ryzhkov, A., & Straka, J. (1999). Cloud microphysics retrieval using S-band dual-polariation radar measurements. *Bull. Amer. Meteor. Soc.*, 381-388.

Wikipedia. (2009, June 20). Retrieved from https://en.wikipedia.org/wiki/Bird_strike#/media/File:Jet_engine_damaged_by_bird_strike.jpg

Wilczak, J. M., Strauch, R. G., Ralph, F. M., Weber, B. L., Merrit, D. A., Jordan, J. R., . . . Riddle, A. C. (1995). Contamination of wind profiler data by migrating birds: characteristics of corrupted data and potential solutions. *J. Atmos. Oceanic Technol.*,, 449-67.

Wilson, J., Weckwerth, T., Vivekanandan, J., Wakimoto, R., & Russel, R. (1994). Boundary layer clear-air radar echoes: origins of echoes and accurracy of derived winds. *J. Atmos. and Ocean. Tech*, 1184-1206.

Zehnder, G. (2014, March 12). *Extension*. Retrieved from Extension: http://articles.extension.org/pages/19198/overview-of-monitoring-and-identification-techniques-for-insect-pests

Zrnic, D., & Ryzhkov, A. (1998). Observations of insects and birds with a polarimetric radar. *IEEE Trans. on Geos. and Remote Sensing*.

Zrnic, D., & Ryzhkov, A. (1999). Polarimetry for weather surveillance radars. *Bull. Amer. Met. Soc.*, 389-406.

Zrnic, D., & Ryzhkov, A. (1999). Polarimetry for weather surveillance radars. *Bull. Amer. Meteor. Soc.*, 381-94.

Zrnic, D., Ryzhkov, A., Straka, J. M., Liu, Y., & Vivekanandan. (2001). Testing a procedure for the automatic classification of hydrometeor types. *J. Atmos. Oceanic Technol.* , 892-913.